

Cite this: *Chem. Sci.*, 2012, **3**, 1903

www.rsc.org/chemicalscience

EDGE ARTICLE

Blended hydrogen atom abstraction and proton-coupled electron transfer mechanisms of closed-shell molecules†

Chunsen Li, David Danovich and Sason Shaik*

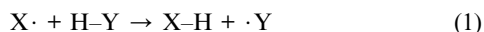
Received 27th January 2012, Accepted 7th March 2012

DOI: 10.1039/c2sc20115a

The paper addresses the surging topic of H-abstractions by closed-shell molecules, such as MnO_4^- , α -methylstyrene, ketones, metal-oxo reagents, *etc.* It is found that in the normal hydrogen atom transfer (HAT) regime, closed-shell abstractors require high barriers for H-abstraction. Under certain conditions a closed-shell abstractor can bypass this penalty *via* a proton-coupled electron transfer (PCET) mechanism. This occurs mainly in the identity reactions, *e.g.* MnO_4^- abstracting a hydrogen atom from MnO_4H^- , but not in the corresponding non-identity reactions with alkanes. The usage of the valence bond (VB) diagram model allows us to characterize the HAT/PCET mechanistic relationship and bridge their reactivity patterns. It is thus shown that in the normal HAT regime, high barriers for closed-shell abstractors occur due to the additional promotion energy that is required in order to create a radical center and “prepare” the abstractor for H-abstraction. Mixing of the PCET states into the HAT states mitigates however these high barriers. The variable HAT/PCET mixing in a reaction series is discussed and its consequences for reactivity are outlined. It is shown that non-identity reactions sample PCET characters that depend, among other factors, on the C–H bond strength of the alkane, and hence may cause the Marcus analysis to produce different identity barriers for the same identity reaction.

Introduction

Hydrogen atom transfer (HAT), eqn (1), is a fundamental process occurring in nature.^{1–12}



While the majority of HAT reactions involve radical abstractors,^{13,14} there has been a growing repertoire of reactions wherein the HAT reaction involves closed-shell abstractors;^{15,16} *e.g.*, α -methylstyrene (α -MS), various ketones, and metal-oxo species such as Cl_2CrO_2 , MnO_4^- , $\text{Mn}(\text{v})\text{O}$. Thus, despite the fact that all these abstractors have no unpaired electrons, they still manage to abstract a hydrogen atom. The notion of closed-shell abstractors has become recently a surging topic, with reports on the efficient H-abstraction reactivity of $\text{Mn}(\text{v})\text{O}$ and $\text{Ru}(\text{iv})\text{O}$ in their singlet states.¹⁶ In view of the fact that in most known $\text{Mn}(\text{v})\text{O}$ systems the reactive state is the open-shell triplet state that is initially an excited state of the abstractor,^{13a,b;17} and the recent report that the

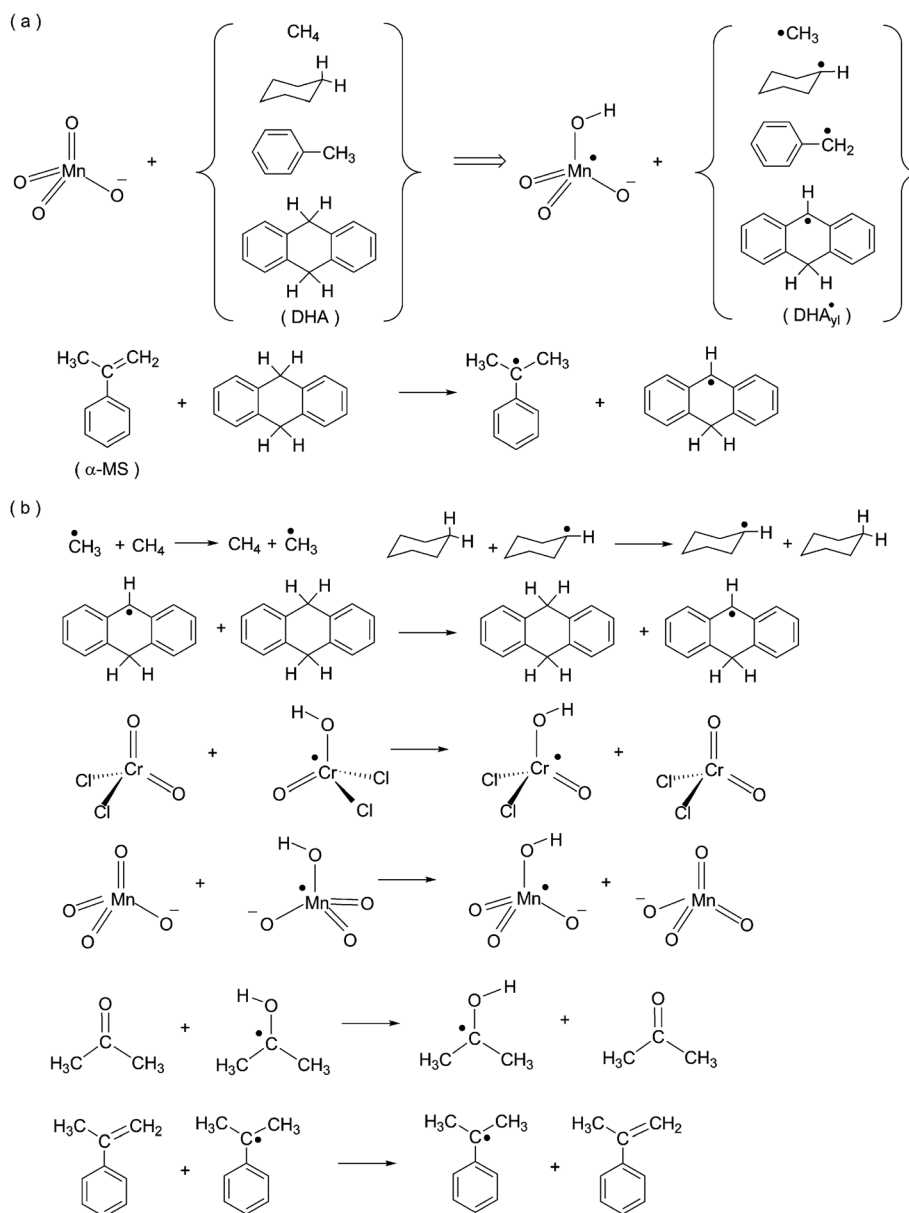
closed-shell abstractor vanadium(v)-oxo is a more sluggish reagent than an analogous open-shell abstractor $\text{Ru}(\text{iv})\text{O}$,¹⁸ it is deemed essential to address the relationship between the open-shell and closed-shell HAT types, and to draw some generalities. This is one goal of this paper.

Another surging topic is the finding that quite a few of the HAT reactions occur *via* the alternative path of concerted proton-coupled electron transfer (PCET).^{19,20} While there is a consensus that in PCET the electron and proton transfer events are separated, different approaches employ different criteria to characterize the mechanism. Our criterion herein is to describe PCET as a process that involves a proton abstraction by the abstractor atom center, while at the same time the electron is relayed to an orbital that is not involved in the H-transfer region.^{19h,i;20} This leads to the question: could all the closed-shell abstractors actually operate by PCET? Even more importantly, the relationship between ‘normal’ HAT and PCET is intriguing, and we would like to outline its consequences in some predictable manner.

To address these questions we performed DFT calculations of the H-abstraction reactions by closed-shell and open-shell abstractors,¹⁵ described in Schemes 1a and b. Scheme 1a shows five reactions; four wherein MnO_4^- abstracts a hydrogen atom from four different alkanes, with decreasing C–H bond strength, methane, cyclohexane, toluene and 9,10-dihydroanthracene (DHA), and the reaction of α -MS with DHA. Scheme 1b shows seven identity self H-exchange reactions, the first three involve

Institute of Chemistry and the Lise-Meitner-Minerva Center for Computational Quantum Chemistry, The Hebrew University of Jerusalem, 91904 Jerusalem, Israel. E-mail: sason@yfaat.ch.huji.ac.il; Fax: +972-2-6584680; Tel: +972-2-6585909

† Electronic supplementary information (ESI) available: Cartesian coordinates of all structures described in this work, tables with *BDE*, *D*, *RE*, ΔE_{ST} , ΔE^\ddagger , and figures of identity of HAT reactions of allyl-/propene and natural orbitals of the triplet TSs of non-identity reactions. See DOI: 10.1039/c2sc20115a



Scheme 1 (a) Non-identity H-abstraction reactions of MnO_4^- with alkanes and the reaction of α -MS with DHA. (b) Identity self H-exchange reactions of the various abstractors.

radical abstractors, and the last four involve closed-shell abstractors. Few other identity reactions of radical abstractors have been studied (*e.g.*, allyl radical and propene, *etc*) but are not depicted in Scheme 1b, and will be mentioned later. The entire data can be found in the electronic supplementary information (ESI†).

The valence bond (VB) diagram model of reactivity²¹ will be used to analyze the computational data and to relate it to experiment. As we shall show, based on a past prediction,^{21b} closed-shell abstractors reacting with alkanes (Scheme 1a) pay an energy penalty of “preparing a radical state” that can perform the HAT. However, it will also be demonstrated that in some of the identity reactions (Scheme 1b), the closed-shell abstractors find a way to evade the energy penalty *via* the PCET mechanism. This dichotomy creates intriguing consequences, such as the

non-unique value of the identity barrier for the closed-shell abstractor derived from the Marcus cross relationship (MCR).^{15e,19b,22,23} It will be argued that this outcome reflects the blending of HAT and PCET characters.

Methods

All calculations were done with the B3LYP functional,²⁴ using the GAUSSIAN 09 package of programs.^{25a} Natural bond orbital (NBO) charge densities were obtained with NBO 5.G.^{25b}

Geometry optimizations were carried out with the all electron 6-311++G** basis set (henceforth, B1).^{26a} All energies include zero-point energy (ZPE) correction. To test the convergence of B3LYP, we used also the Def2-TZVP basis set (B2), which is an extended all-electron basis set designed for DFT calculations.^{26b}

The calculations showed deviations of barrier by ~ 1.0 kcal mol⁻¹, and of even less than that for reactivity factors, such as the singlet–triplet excitations and bond dissociation energies (*BDEs*), needed for the application of the VB model.^{21,27} In the case of the ketone/ketyl reaction (Scheme 1b),^{15j} we used CCSD(T) with correlation consistent basis sets,^{26c} to estimate the *BDE* of the O–H bond of the ketyl radical (see Table S1, ESI†).

Since we are interested in the nature of H-abstraction process, the investigation was limited to the H-abstraction step (see Fig. 1 later) starting from the reactant cluster (**RC**) and ending in the H-abstraction intermediate (**I_H**). The follow-up steps were not studied.

All the non-identity reactions in Scheme 1a start as closed-shell singlet state reactants, but end up with open-shell singlet-diradical states. As such, one must be careful to ascertain that these reactions do not exhibit non-physical effects due to self-interaction error (SIE).²⁸ Using the diagnosis in ref. 28, we found that the reactions in Schemes 1a do not exhibit these effects and additionally, the computed barriers match experiment whenever available.

We also tested the option that the reactions in Scheme 1a pass *via* the closed-shell transition states (TSs) or *via* triplet TSs. For example, for the reaction of MnO₄⁻ with methane, we found that the closed-shell TS lies near to the open-shell TS, and is only 3.7/4.1 kcal mol⁻¹ higher in energy (optimized/single point closed-shell TS calculation on the geometry of the open-shell TS). Similar results were found for all the reactions in Scheme 1a; the closed-shell TSs were 0.5–4.0 kcal mol⁻¹ higher than the open-shell ones. To avoid any bias for one set or the other, we shall display two sets of barriers, one going through the lower-energy open-shell TS, the other through the slightly higher closed-shell TS. In contrast, the triplet transition states were significantly higher, 5.1–13.3 kcal mol⁻¹ higher than the open-shell singlet TSs (see Table S4, ESI†), and were accordingly ruled out as mediators for these reactions. The reaction energies (from **RC** to **I_H**) for all these processes were well within 1 kcal mol⁻¹ from the difference in the computed *BDEs* of the C–H and ·MnO₃O–H⁻ bonds, and hence these values were used in the analyses for both sets.

The reactions in Scheme 1b involve open-shell to open-shell transformations and are hence less susceptible to SIE effects. Indeed, all of the identity reactions showed no obvious signs of SIE.²⁸ The identity reaction MnO₄⁻/MnO₄H⁻· was studied by adding K⁺ counter ions in order to generate an RC. In the absence of the counter ions the electrostatic repulsion prevented the approach of the reactants. It was verified that the removal of the counter ions from the RC and TS, followed by partial optimization keeping the H···O distance in the [O₃MnOH···OMnO₃]²⁻ RC fixed, and fully optimizing the TS, produced a rather similar energy barrier. Hence, the counter ions simply mask the electrostatic repulsion, but otherwise do not affect the activation associated with the H-abstraction.

Results

Barrier data

Fig. 1 shows the generic energy profile for the reactions in Schemes 1a and b. Initially the reactants form a loose **RC**. In the non-identity case, the H-abstraction leads to the formation of the H-abtracted intermediate, **I_H**, which is a singlet-diradical for all the cases. In the identity reactions, the reactant and product clusters are mirror images and are labeled as **RC** and **PC**.

Tables 1 and 2 collect barriers, reaction energies, and available experimental data. The two sets of barriers correspond to the open-shell (OS) and closed-shell (CS) TSs. Added to Table 1 (entries 1b and 3b) are previous data,²⁹ and while the original paper does not specify it, the barrier data seem to correspond to the closed-shell option. It is seen that for three of the reactions (entries 3–5), for which experimental data are available,^{15e-h} the DFT barriers and thermodynamic driving force quantities match experimental values. Furthermore, as found experimentally, the barriers in Table 1 reflect the Bell–Evans–Polanyi (BEP) principle,³⁰ decreasing as the reaction driving force becomes less endothermic.^{15e-h}

Table 2 reports the calculated and experimental barriers for the identity reactions in Scheme 1b. The experimental barriers for these reactions are given whenever available as $\Delta G_{\text{exp}}^{\ddagger}$.

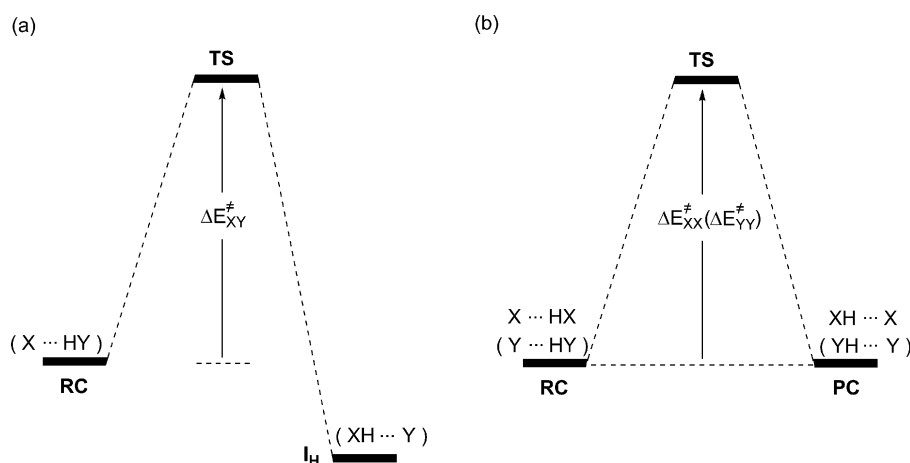


Fig. 1 Generic energy profiles, showing barriers and reaction energies for H-abstraction during (a) non-identity reactions (the reaction energy is the difference between the **I_H** and **RC** energies), and (b) identity reactions. **RC** and **PC** are reactant and product clusters, respectively, and **I_H** is the H-abtracted intermediate for the non-identity process.

Table 1 B3LYP/B1 calculated and experimental barriers and thermodynamic driving forces (kcal mol⁻¹) for the non-identity reactions in Scheme 1a^a

X	Y-H	$\Delta E^\ddagger(\text{OS})/\Delta E^\ddagger(\text{CS})$	$\Delta E_{\text{RC-IH}}$	$\Delta H^\ddagger_{\text{exp}}(\Delta G^\ddagger_{\text{exp}})$	$\Delta H^\circ_{\text{exp}}{}^f$
(1a) MnO ₄ ⁻	CH ₄	27.3/31.4	23.4		25.0
(1b) MnO ₄ ⁻	CH ₄	32.3 ^b	24.3 ^b		
(2) MnO ₄ ⁻	C ₆ H ₁₂	23.3/27.3	16.4		19.3
(3a) MnO ₄ ⁻	PhCH ₃	20.0/21.6	7.0	21.0 ± 1.0 (26.0 ± 1.0) ^c	9.9
(3b) MnO ₄ ⁻	PhCH ₃	21.8 ^b			
(4) MnO ₄ ⁻	DHA	14.6/15.1	-5.2	13.8 ± 1.0 (19.0 ± 2.0) ^c	-2.0
(5) α-MS	DHA	32.6/33.1	26.6	35.9 ± 1.4 (44.7 ± 1.4) ^d (41.0) ^e	31.5

^a All values are corrected by ZPE. See Fig. 1a for definitions. ^b From ref. 29. ^c From ref. 15e-g. ^d From ref. 15h. ^e $\Delta G^\ddagger_{\text{exp}}$ value, scaled to 298 K. ^f Using BDEs.

($\Delta H^\ddagger_{\text{exp}}$), respectively.^{15,31-33} The experimental identity barriers in entries 1 and 6 were directly derived from kinetics.^{15,31} It is seen that the DFT barrier for the methyl-radical/methane self H-exchange is very close to the experimental activation energy datum. The corresponding $\Delta G^\ddagger_{\text{exp}}$ datum is, as expected, higher by ~5–6 kcal mol⁻¹, due to the entropic contribution associated with the loss of degrees of freedom upon association ($-T\Delta S^\ddagger_{\text{exp}}$, $T = 298$ K). Generally speaking, DFT seems to be quite reliable for calculating barriers of identity H-abstraction reactions between alkyl radicals and alkanes. For example, the B3LYP/B1 identity barrier^{20a} of 16.5 kcal mol⁻¹ for PhCH₂·/PhCH₃ is reasonably close to the experimental enthalpic barrier, 18.7 kcal mol⁻¹,³³ and as expected, the corresponding $\Delta G^\ddagger_{\text{exp}}$ datum is about ~5 kcal mol⁻¹ higher, 23.4 kcal mol⁻¹. In this respect, it is also gratifying to note that the DFT value in entry 6 is close to but lower than the experimentally determined free energy of activation for analogous reactions.^{15f}

The other “experimental” identity barriers, in entries 3–5, were extracted³² by using the MCR^{22,23} analysis in eqn (2a) and (2b) (see comments in ESI†).

$$\Delta G^\ddagger_{\text{XY}} = \Delta G_0^\ddagger + 0.5\Delta G_{\text{rp}} + \Delta G_{\text{rp}}^2/16\Delta G_0^\ddagger \quad (2a)$$

$$\Delta G_0^\ddagger = 1/2[\Delta G^\ddagger_{\text{XX}} + \Delta G^\ddagger_{\text{YY}}] \quad (2b)$$

The MCR procedure involves first, using eqn (2a), the dissection of the barrier $\Delta G^\ddagger_{\text{XY}}$ for a non-identity reaction to yield an intrinsic barrier, ΔG_0^\ddagger . In turn, ΔG_0^\ddagger is expressed as an

average of two identity barriers as in eqn (2b). Knowing one of these identity barriers enables one to extract the other. The extracted identity barriers are assumed to carry over from one reaction to the other (see ESI†). Thus, the MCR extracted identity barrier (entry 3), 31.5 kcal mol⁻¹, for the reaction of DHA_{yl}·-radical/DHA,^{32a,b} was used by us in eqn (2) together with the barrier for the non-identity reaction of MnO₄⁻ with DHA,^{15g} and the corresponding bond dissociation free energies^{32b,d} which yield $\Delta G_{\text{rp}}(\text{MnO}_4^-/\text{DHA}) = -5.7$ kcal mol⁻¹, to derive the barrier datum, 11.4 kcal mol⁻¹, for MnO₄⁻/MnO₄H· (entry 4). Note that the MCR-based identity free energy barrier for DHA_{yl}·-radical/DHA, appears too high, considering barriers of other alkyl/alkane reactions discussed above. Thus, assuming an analogy to PhCH₂·/PhCH₃, for which $\Delta G^\ddagger(\text{PhCH}_2\cdot/\text{PhCH}_3) = 23.4$ kcal mol⁻¹, would predict for MnO₄⁻/MnO₄H·, an identity free energy barrier, ~19.6 kcal mol⁻¹ (see comments in ESI†).

Entry 5, in Table 2, is seen to involve two different “experimental” values for the identity barrier of Cl₂CrO₂/Cl₂CrO₂H·, which are extracted from MCR analyses of two different reactions. The first and lower value was extracted from the reaction of Cl₂CrO₂ with PhCH₃,^{15f} and the second one from the reaction of Cl₂CrO₂ with cyclohexane.^{15c,d} The B3LYP calculated identity barrier is close to the smaller free energy barrier datum. Finally, in entry 7, the MCR extracted identity barrier (from data for the non-identity reaction of α-MS with DHA^{15h}) is significantly smaller than the directly calculated DFT value. As we shall see later despite the inherent uncertainties in experimental MCR

Table 2 B3LYP/B1 calculated and experimentally derived barriers (kcal mol⁻¹) for the identity reactions in Scheme 1b^a

X	X-H	$\Delta E^\ddagger_{\text{XX,B3LYP}}$	$\Delta G^\ddagger_{\text{exp,XX}} (\Delta H^\ddagger_{\text{exp,XX}})$
(1) CH ₃ ·	CH ₄	14.6	20.0 (14.7) ^b
(2) C ₆ H ₁₁ ·	C ₆ H ₁₂	15.0 (ee)/15.6 (aa) ^c	
(3) DHA _{yl} ·	DHA	17.2	31.5 ^d
(4) MnO ₄ ⁻	MnO ₄ H·	11.6	11.4 ^e
(5) Cl ₂ CrO ₂	Cl ₂ CrO ₂ H·	11.5	12.9 (4.7)/30.0 (21.2) ^f
(6) (CH ₃) ₂ CO	(CH ₃) ₂ COH·	10.3	12.6 ^g
(7) Ph(CH ₃)C=CH ₂	Ph(CH ₃) ₂ C·	23.2	(15.6) ^h

^a See Fig. 1b for notations of the barriers. ^b From ref. 31. ^c For equatorial/equatorial and axial/axial C-H bonds. ^d Using MCR analysis (eqn (2)). The $\Delta G^\ddagger_{\text{exp,XX}}$ is derived from the Eyring equation using the reported^{32a,b} rate constant $5 \times 10^{-11} \text{ M}^{-1} \text{ s}^{-1}$ ($T = 298$ K), extracted from MCR analysis of the reaction, Fe^{III}(Hbim) + DHA. ^e Using the data in *d* and $\Delta G_{\text{rp}} = -5.7$ kcal mol⁻¹ generates this identity barrier. The reported^{32c} MCR estimated rate constant = $2 \times 10^6 \text{ M}^{-1} \text{ s}^{-1}$. ^f Using the MCR analysis of the reactions, Cl₂CrO₂ + PhCH₃/Cl₂CrO₂ + C₆H₁₂, respectively. See ref. 15f for data. The experimental identity barrier for PhCH₂·/PhCH₃ is from ref. 33. The identity barrier for C₆H₁₁·/C₆H₁₂ was estimated in ref. 21e to be 20.2 (13.8) kcal mol⁻¹. ^g From ref. 15j. ^h From MCR analysis, using the experimental ΔH^\ddagger and ΔH data for the non-identity reaction, Ph(CH₃)C=CH₂/DHA, in entry 5 (Table 1), and the computed $\Delta E^\ddagger_{\text{YY}}$ (Y = DHA) = 17.2 kcal mol⁻¹.

analyses, the observation of different identity barriers extracted from the application of the MCR procedure to different non-identity process may not be an artifact, and may represent an HAT/PCET mechanistic blend, which is different for different reactions.

Using the B3LYP/B1 barriers and thermodynamic driving forces in Tables 1 and 2, one can perform an MCR analysis (eqn (2a) and (2b)) and derive intrinsic barriers from the DFT calculated data. The so-obtained intrinsic barriers can in turn yield the identity barriers of the abstractors, ΔE_{XX}^\ddagger , based on known values for the alkyl-radical/alkane reactions (Table 2). Since the MCR analysis is sensitive to the barrier values, we used only our computationally uniform set of B3LYP/B1 barriers from Table 1. We recall that each reaction has a barrier calculated with the open-shell option and a slightly higher one calculated with the closed-shell option. To avoid any bias in the conclusions, we performed the MCR analysis on both barriers sets. Table 3 collects the results of this MCR analysis. In the first column of numerical values, we show the intrinsic barriers, ΔE_0^\ddagger values (eqn (2a)), and in the following column we show the identity barriers for the abstractor's self H-exchange reaction, ΔE_{XX}^\ddagger , derived from eqn (2b). The last column of numerical values shows the corresponding ΔE_{XX}^\ddagger (B3LYP) values, obtained from direct B3LYP/B1 calculations of the self H-exchange reactions.

The first four entries of the ΔE_{XX}^\ddagger (eqn (2b)) column, in Table 3, all refer to the same self-exchange reaction, $\text{MnO}_4^-/\text{MnO}_4\text{H}^-$. No matter which barrier set we use in the MCR analysis, the so-extracted identity barrier for the $\text{MnO}_4^-/\text{MnO}_4\text{H}^-$ identity reaction depends on the non-identity reaction used for the analysis. Using the open-shell derived barriers, the resulting $\Delta E_{XX}^\ddagger(\text{MnO}_4^-/\text{MnO}_4\text{H}^-)$ values obtained from the reactions of MnO_4^- with CH_4 and with C_6H_{12} are close to the directly calculated DFT barrier, and are significantly lower than the values obtained from the reactions with PhCH_3 and DHA , where the C–H bonds are weaker. On the other hand, using the barriers derived from the closed-shell option gave higher $\Delta E_{XX}^\ddagger(\text{MnO}_4^-/\text{MnO}_4\text{H}^-)$ values for CH_4 and with C_6H_{12} . Finally, the closed-shell barriers for the closed-shell optimized TSs (not shown in Table 3), gave the same trend with $\Delta E_{XX}^\ddagger(\text{MnO}_4^-/\text{MnO}_4\text{H}^-)$ values varying between 27.0 and 18.1 kcal mol⁻¹. Thus, in all sets, the extracted identity barrier for the identity process $\text{MnO}_4^-/\text{MnO}_4\text{H}^-$ differs from one reaction to the other, and most values are higher than the directly calculated identity barrier. This variation reminds the analysis of the experimental barriers in entry 5 in Table 2, where different

non-identity reactions yielded different identity barriers for the same identity reaction, $\text{Cl}_2\text{CrO}_2/\text{Cl}_2\text{CrO}_2\text{H}^\cdot$ from two different reactions. Another interesting feature is seen in entry 5, where the MCR-based identity barrier for α -MS abstracting an H from cumyl \cdot radical is 16.6/17.8 kcal mol⁻¹. These values are very close to the $\Delta H_{XX}^\ddagger(\alpha\text{-MS}/\text{cumyl}\cdot)$ value of 15.6 kcal mol⁻¹ extracted by MCR analysis of the experimental data^{15h} (Table 2, entry 7). By contrast, the directly computed value (B3LYP/B1) is higher, 23.2 kcal mol⁻¹. The origins of this dichotomy will be analyzed in the discussion section.

Transition state features

Fig. 2 shows the transition states for the HAT reactions of the open-shell alkyl radicals. Fig. 2 also includes key geometric features, spin and charge density distributions, and plots of the singly occupied natural orbital (NO) in the TS. The three TSs are quite similar, all having a virtually linear $\text{C}\cdots\text{H}\cdots\text{C}$ moiety with CH distances in the range of 1.347–1.377 Å, their spin distribution involves large positive spin densities on the two alkyl moieties, and a small negative density on the middle H moiety, typical of three-electron/three-center delocalized species.^{21c,34} The singly occupied NO in all the TSs is a non-bonding orbital with a node on the H in transit, thus further revealing the expected electronic structure of typical to normal HAT TSs with three-electron/three-center delocalization.

Fig. 3 shows the four TSs for the identity reactions where the abstractor is a *closed*-shell molecule. The three TSs in Fig. 3a–c possess $\text{O}\cdots\text{H}\cdots\text{O}$ moieties in the HAT region. In all of the three structures the $\text{O}\cdots\text{H}$ distances are similar, 1.194–1.195 Å, the total spin density on the $\text{O}\cdots\text{H}\cdots\text{O}$ transit region is rather small, while the charges strongly alternates, for example, $-0.62/+0.47/-0.62$ for the TS in Fig. 3a. Furthermore, in all of the cases the singly occupied NO is not in the transit region. In the cases of the metal-oxo abstractors (Fig. 3a and b), the electron is in an orbital made from a combination of the d orbitals (with antibonding character from the other oxo ligands) on the metal-centers, and in the case of the ketone/ketyl reaction in Fig. 3c, the singly occupied NO is positive combination of the π^*_{CO} (mostly of $2p_{\pi}(\text{C})$ character) orbitals of the CO moieties flanking the H in transit. In the 4th TS (Fig. 3d) corresponding to the reaction of α -MS and cumyl \cdot radical, the C–H distances are quite long, 1.391 Å, the spin density in the $\text{H}_2\text{C}\cdots\text{H}\cdots\text{CH}_2$ transit region is small, while the charges are relatively small ($-0.12/+0.24/-0.12$). The singly occupied orbital in Fig. 3d spans mostly the benzylic

Table 3 Intrinsic and identity barriers (kcal mol⁻¹), extracted by application of eqn (2a) and (2b) on the B3LYP/B1 barriers for non-identity reactions, $\text{X} + \text{H}-\text{Y} \rightarrow \cdot\text{X}-\text{H} + \text{Y}\cdot$, shown alongside B3LYP/B1 calculated identity barriers for $\text{X} + \text{H} - \text{X} \cdot \rightarrow \cdot\text{X} - \text{H} + \text{X}$

X	H–Y	ΔE_0^\ddagger (eqn (2a)) ^a	ΔE_{XX}^\ddagger (eqn (2b)) ^{a,b}	ΔH_{XX}^\ddagger (B3LYP)
(1) MnO_4^-	CH_4	13.0/17.8	11.4/21.0	11.6 (~15) ^c
(2) MnO_4^-	C_6H_{12}	13.9/18.2	12.2/20.8	11.6 (~15) ^c
(3) MnO_4^-	PhCH_3	16.3/17.9	16.1/19.3	11.6 (~15) ^c
(4) MnO_4^-	DHA	17.1/17.6	17.0/18.0	11.6 (~15) ^c
(5) α -MS	DHA	16.6/17.2	16.6/17.8	23.2

^a Calculated using the MCR analysis (eqn (2a) and (2b)). The two values reported for each entry correspond to MCR analysis of the $\Delta E_0^\ddagger(\text{OS})/\Delta E_0^\ddagger(\text{CS})$ values taken from Table 1. ^b ΔE_{XX}^\ddagger values were calculated from the intrinsic barriers, ΔE_0^\ddagger (eqn (2b)) using ΔE_{YY}^\ddagger values from Table 2 ($\text{Y} = \text{CH}_3$, C_6H_{11} , DHA_y and α -MS/cumyl \cdot). For $\text{Y} = \text{PhCH}_2$ from ref. 20a. ^c Directly computed for $\text{MnO}_4^- \cdot \text{K}^+/\text{MnO}_4\text{H}^- \cdot \text{K}^+$ using B3LYP/B1 (see Table 2). The value in parentheses is an approximate value obtained by removal of the counter ions while performing constrained optimization (see Methods).

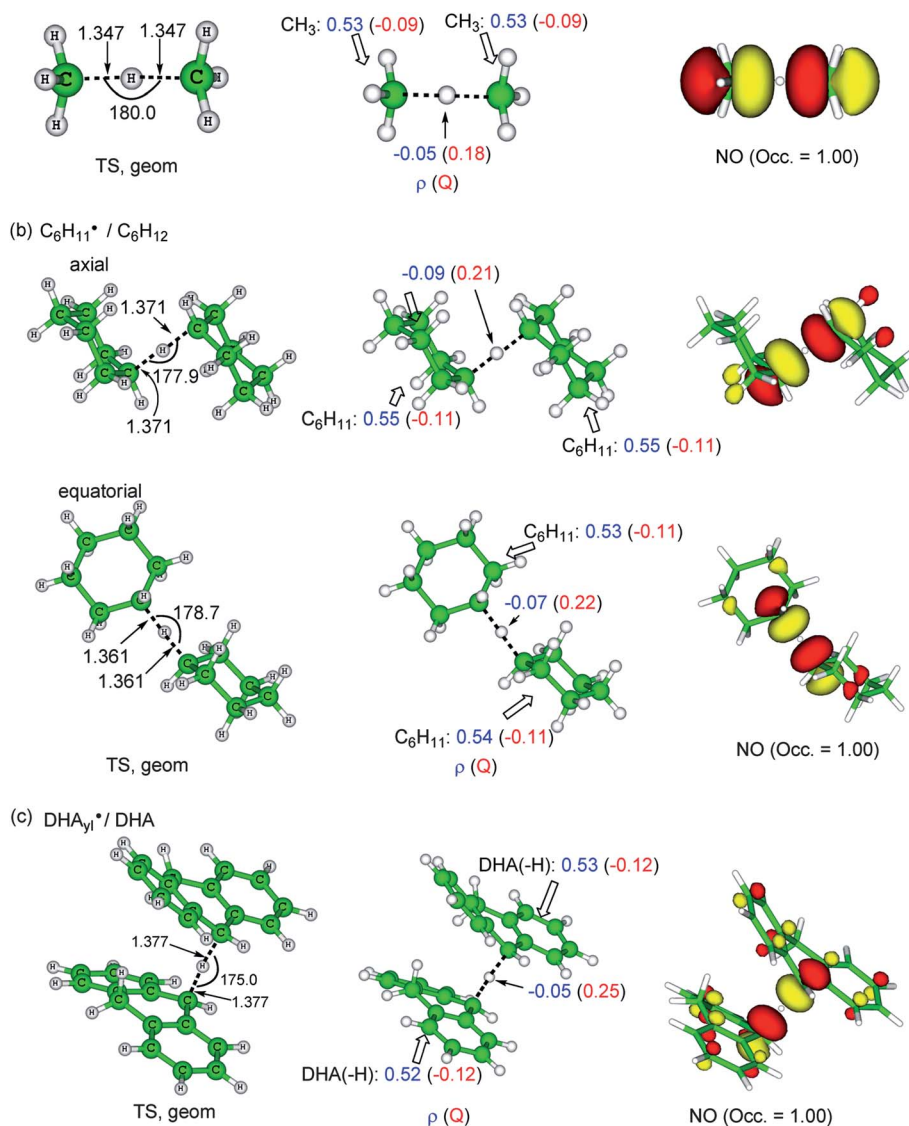


Fig. 2 Key geometric features, group spin densities (ρ), NBO charges (Q), and the singly occupied natural orbital (NO) for the identity HAT reactions of the following pairs; (a) $\text{CH}_3\cdot/\text{CH}_4$, (b) $\text{C}_6\text{H}_{11}\cdot/\text{C}_6\text{H}_{12}$ (axial-axial and equatorial-equatorial), and (c) $\text{DHA}_{y1}\cdot^*/\text{DHA}$.

carbons with a contribution on the H in transit, which is not reminiscent of the “normal” HAT orbitals in Fig. 2. Clearly these four self H-exchange TSs that mediate the HAT of closed-shell abstractors are entirely different than the TSs for the radical abstractors in Fig. 2. Three of them look like proton transfers in the transit region, along with an odd electron transfer through another set of orbitals, namely PCET processes.^{19h,i;20} The fourth one is certainly not a PCET TS, but what is it then?

Fig. 4 shows the open-shell optimized TS species for the non-identity reactions of the closed-shell anion MnO_4^- (parts a–c) and of $\alpha\text{-MS}$ (part d). Fig. 4 also includes geometric features, spin and charge density distributions, and plots of the two singly occupied corresponding orbitals³⁶ (COs) in the TS. These COs are obtained by transforming the corresponding NOs that are fractionally occupied to singly occupied ones (for the NOs of the triplet TSs see Fig. S2 in ESI†).

Comparison of these non-identity reactions to the identity processes in Fig. 3 reveals striking differences. Thus, whereas the

spin density and singly occupied orbitals of $\text{MnO}_4^-/\text{MnO}_3\text{OH}^-$ (Fig. 3a) are not involved with the $\text{O}\cdots\text{H}\cdots\text{O}$ transit region and are typical of PCET mechanisms, for the non-identity reactions of MnO_4^- (Fig. 4a–c) those features are entirely different. For example, Fig. 4a reveals that the TS for $\text{MnO}_4^-/\text{C}_6\text{H}_{12}$ involves typical HAT features; alternating spin density distribution in the transit region $\text{O}\cdots\text{H}\cdots\text{C}$,³⁴ with large densities on the atoms flanking the H, and two singly occupied orbitals, one is largely an MnO d-type orbital (π^*_{MnO}), and the other is spanned over the transit region with a node on the H atom in transit (ϕ^*_{OC}). In the closed-shell TS species, the latter orbital is doubly occupied, while the similar one with the greater d-type (π^*_{MnO}) contribution is vacant. Similar features are noticeable in all the other non-identity processes in Fig. 4; their two singly occupied orbitals possess each a node between the carbon-centered hybrid and the π or π^* d-type orbitals of MnO (Fig. 4b, c), or the $\text{C}=\text{C}$ π and π^* orbitals of $\alpha\text{-MS}$ (Fig. 4d). All these TSs resemble the standard HAT reactions in Fig. 2. Note however, that the charge

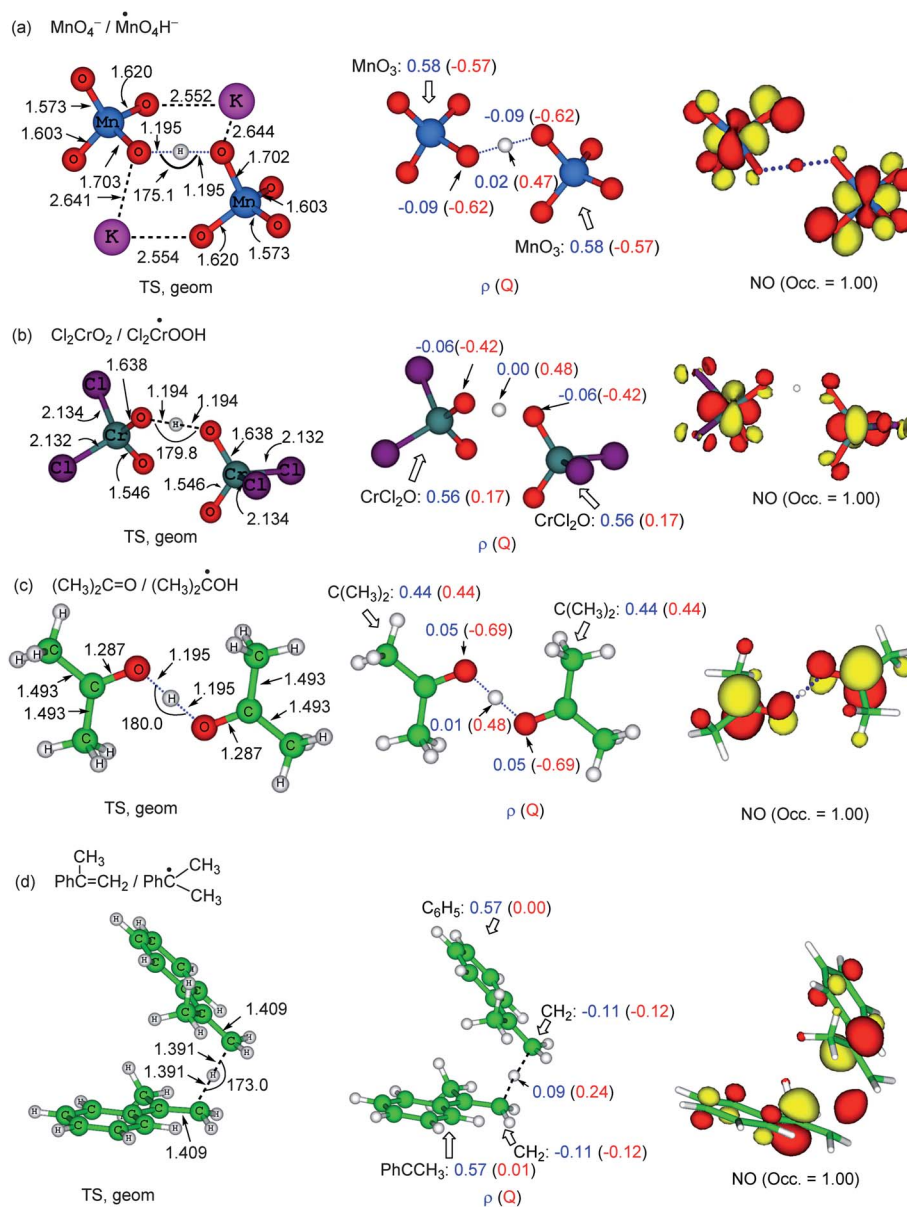


Fig. 3 Key geometric features, spin densities (ρ), NBO charges (Q), and the singly occupied natural orbital (NO) for the identity HAT reactions of the following pairs; (a) $\text{MnO}_4^-/\text{MnO}_3\text{OH}\cdot$, (b) $\text{Cl}_2\text{CrO}_2/\text{Cl}_2\text{CrOOH}\cdot$, (c) $(\text{CH}_3)_2\text{C}=\text{O}/(\text{CH}_3)_2\text{C}\cdot\text{OH}$, and (d) $\text{Ph}(\text{CH}_3)\text{C}=\text{CH}_2/\text{PhC}(\text{CH}_3)_2\cdot$.

distribution is still alternating in the transit region, and exhibits a significant proton transfer character (see *e.g.*, Q_{H} values), which is variable for the different processes of MnO_4^- . Clearly, whereas the identity processes of the closed-shell abstractors (Fig. 3) are ‘normal’ PCET, the non-identity processes of these abstractors (Fig. 4) become largely HAT types with some PCET characters, which is mostly apparent from the group charges at the transit region. This issue will be discussed in the next section.

Discussion

A. Electronic structures of HAT and PCET mechanisms

Let us start the discussion by providing first, in Scheme 2, simplified orbital pictures of the TSs.^{19d,e;20} Scheme 2a describes

a HAT process, where the $\text{X}\cdots\text{H}\cdots\text{Y}$ moiety in the transition state involves three electrons, one contributed by the $\text{X}\cdot$ radical center and two by the $\text{H}-\text{Y}$ bond pair, hence producing a three-electron/three-center TS. The characteristic orbitals of such a TS are the doubly occupied bonding orbital along the axis $\text{X}\cdots\text{H}\cdots\text{Y}$, ϕ_{σ^+} , and the singly-occupied non-bonding-type orbital, ϕ_{σ^-} , having a node on the H atom in transit. Such a TS typifies the alkyl-radical/alkane reactions in Fig. 2.

Scheme 2b shows an alternative manner for H atom transfer. Here the abstractor is the closed-shell ketone, $\text{R}_2\text{C}=\text{O}$, while the H atom donor molecule is the corresponding ketyl radical, $\text{R}_2\text{C}-\text{OH}\cdot$, that possesses an odd electron in an antibonding π^* orbital composed largely of $2p_{\pi}(\text{C})$ with a smaller contribution from $2p_{\pi}(\text{O})$. As can be seen from Scheme 2b, in the TS the abstractor conserves the π -bond and utilizes instead an

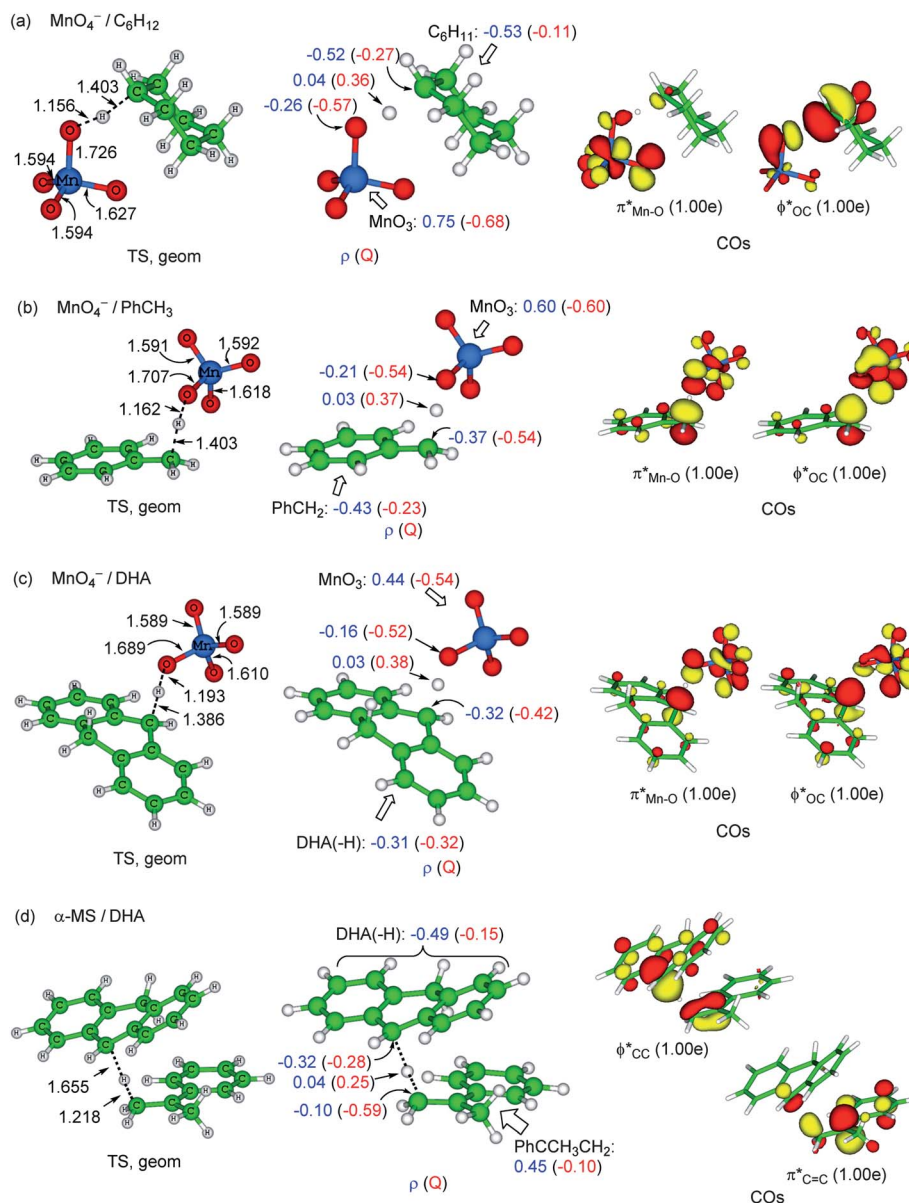


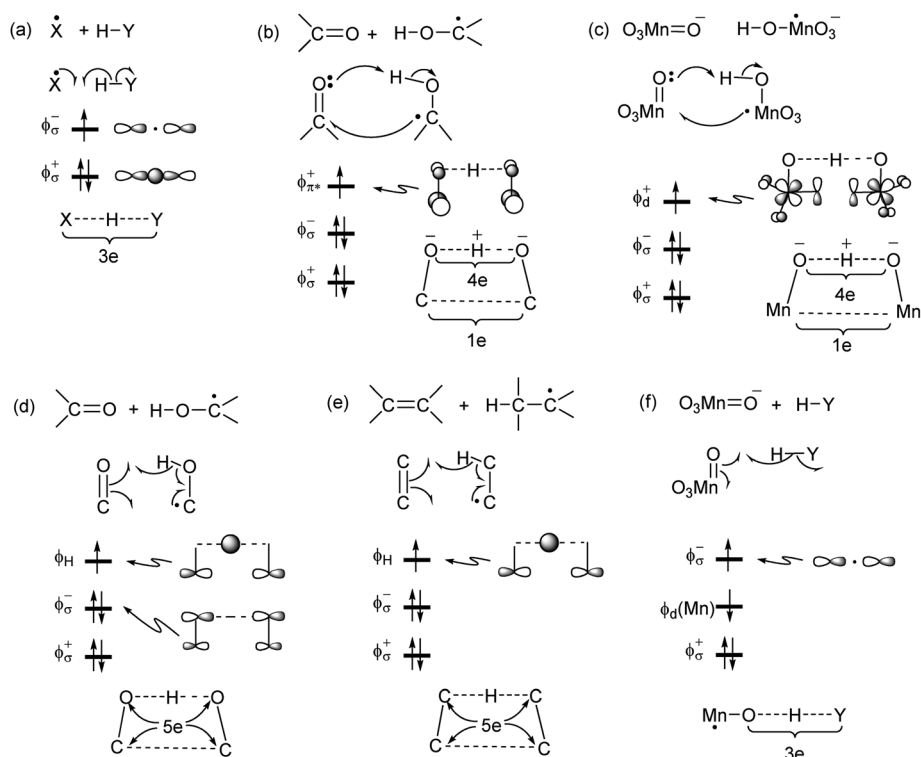
Fig. 4 Key geometric features, spin densities (ρ), NBO charges (Q), and the singly occupied corresponding orbitals (COs) for the non-identity HAT reactions of the following pairs; (a) $\text{MnO}_4^-/\text{C}_6\text{H}_{12}$, (b) $\text{MnO}_4^-/\text{PhCH}_3$, (c) $\text{MnO}_4^-/\text{DHA}$ and (d) $\alpha\text{-MS}/\text{DHA}$. For simplicity we keep the same labels for the COs in parts (a)–(c).

electron-pair on the oxo moiety as a base that abstracts the proton from the O–H bond of the $\text{R}_2\text{C}\text{-OH}\cdot$ radical, while the odd electron is transferred from one π^* orbital to the other, thus being located in their positive combination, ϕ_{π^*} in the TS. The reaction between the closed-shell MnO_4^- abstractor and the H atom donor radical $\text{MnO}_3\text{OH}\cdot$, in Scheme 2c, follows precisely the same route, and the orbital that accommodates the single electron is composed here of the combination of the d orbitals on the Mn centers, with antibonding contributions from the oxygen ligands. The reaction of Cl_2CrO_2 with $\text{Cl}_2\text{CrO}_2\text{H}\cdot$ conforms to Scheme 2c.

The $\text{O}\cdots\text{H}\cdots\text{O}$ transit moieties in the TSs in Schemes 2b and c look therefore like proton abstraction moieties, with four electrons delocalized over three centers, with two electrons in each of the ϕ_{σ^+} and ϕ_{σ^-} orbitals. At the same time, the odd electron is

transferred between the low-lying antibonding orbitals. Such TSs typify the identity reactions of the closed-shell abstractors in Fig. 3a–c, and are referred to as PCET TSs, since they involve proton transfer in the $\text{O}\cdots\text{H}\cdots\text{O}$ region coupled to an “electron transfer” between orbitals that lie off this region. Thus the electron and proton transfer events are separated “in space”, albeit being concerted, as commonly understood for the PCET mechanism.^{19,20}

Scheme 2d depicts the orbitals for the HAT process, which is alternative to the PCET described in Scheme 2b. Here the closed-shell ketone decouples the π -bonding electrons of the $\text{C}=\text{O}$ bond such that in the TS we have in total five electrons delocalized over five centers. The singly occupied orbital of such a five-electron/five-center TS is labeled in Scheme 2d as ϕ_{H} , and is shown to possess a large contribution on the H in transit. The alternative



Scheme 2 Key orbitals in the transition states in various H-abstraction mechanisms. (a) A normal HAT mechanism *via* an $X\cdots H\cdots Y$ three-electron/three-center TS. (b) A PCET mechanism in the reaction of ketone with a ketyl radical with a four-electron/three-center proton-abstraction moiety and 1e-delocalization between π^* orbitals centered on the carbons. (c) A PCET mechanism in the reaction of MnO_4^- and $MnO_3OH\cdot$. (d) An alternative HAT mechanism in the reaction of ketone with a ketyl radical, *via* a five-electron/five-center TS, having a single electron in a ϕ_H orbital, with large contribution on the H in transit and small ones from the d-orbitals of the two Mn atoms. Scheme 2e shows that this type of HAT mechanism in fact occurs in our calculations between the closed shell α -MS abstractor and the cumyl \cdot radical, and the singly occupied ϕ_H orbital is precisely the one shown above in Fig. 3d for this reaction. (e) A HAT mechanism with a five-electron/five-center TS in the reaction of an olefin with an alkyl radical. (f) A HAT mechanism in the non-identity reaction of MnO_4^- with an alkane $H-Y$ (only the oxyl contribution is shown for the MnO_4^- orbital).

HAT process for the reaction of the closed-shell MnO_4^- abstractor with $MnO_3OH\cdot$ would be precisely analogous to the description in Scheme 2d. In this case too, the abstractor will have to decouple the π -bonding electrons of the $Mn=O$ bond, and create a five-electron/five-center TS, having a single electron in a ϕ_H orbital, with large contribution on the H in transit and small ones from the d-orbitals of the two Mn atoms. Scheme 2e shows that this type of HAT mechanism in fact occurs in our calculations between the closed shell α -MS abstractor and the cumyl \cdot radical, and the singly occupied ϕ_H orbital is precisely the one shown above in Fig. 3d for this reaction.

Finally, Scheme 2f shows the non-identity reaction between the closed-shell MnO_4^- abstractor and an alkane, $H-Y$. It is seen that here the abstractor must decouple its $\pi_{Mn=O}$ electrons and participate in a normal HAT. The singly occupied orbitals will be then, the common HAT orbital ϕ_{σ}^{-} (on the $O\cdots H\cdots Y$ region) and a d-type π^* orbital largely on MnO ($\phi_d(Mn)$). This is precisely the electronic structure for the TSs of all the non-identity reactions of MnO_4^- with the various alkanes in Fig. 4a–c, and is also the case for the reaction of α -MS with DHA in Fig. 4d (where the second orbital is π^* on α -MS).

It is apparent from Scheme 2 that H-abstraction has two possible mechanisms, HAT and PCET. Simple radicals abstract an H atom *via* the three-electron/three-center HAT mechanism as in Scheme 2a. However, the identity reactions of ketone/ketyl \cdot , $MnO_4^-/MnO_3OH\cdot$, and $Cl_2CrO_2/Cl_2CrO_2H\cdot$ transpire

via the PCET mechanism as in Schemes 2b and c, while in the non-identity reactions with alkanes, these closed-shell abstractors select the regular HAT mechanisms, as in Scheme 2f. When the closed-shell abstractor is a double bond of an olefin, as in Scheme 2e, the process occurs by a five-electron/five-center HAT mechanism. It is a good place therefore to discuss the mechanistic choices for the various reactions we investigated in the present study. In so doing, we shall show that a HAT/PCET mechanistic blending could be responsible for the non-unique identity barrier extracted by the MCR analysis of different non-identity reactions of closed-shell abstractors. This will be done by means of VB theory.^{21,27} Our discussion of the PCET mechanism will not cover the non-adiabatic features.^{19d,e}

B. Valence bond analysis of HAT and PCET mechanisms

The VB state correlation diagram (VBSCD) uses state correlations to model the formation of the transition state and barrier for elementary steps.²¹ Since it has been described in great detail before, we shall simply apply it herein to the HAT and PCET mechanisms.

VB modeling of HAT for identity reactions. Fig. 5 depicts the VBSCD for identity reactions; Fig. 5a describes the generic HAT mechanism for a simple radical $X\cdot$, while Fig. 5b describes an *assumed* HAT for a closed-shell abstractor represented by

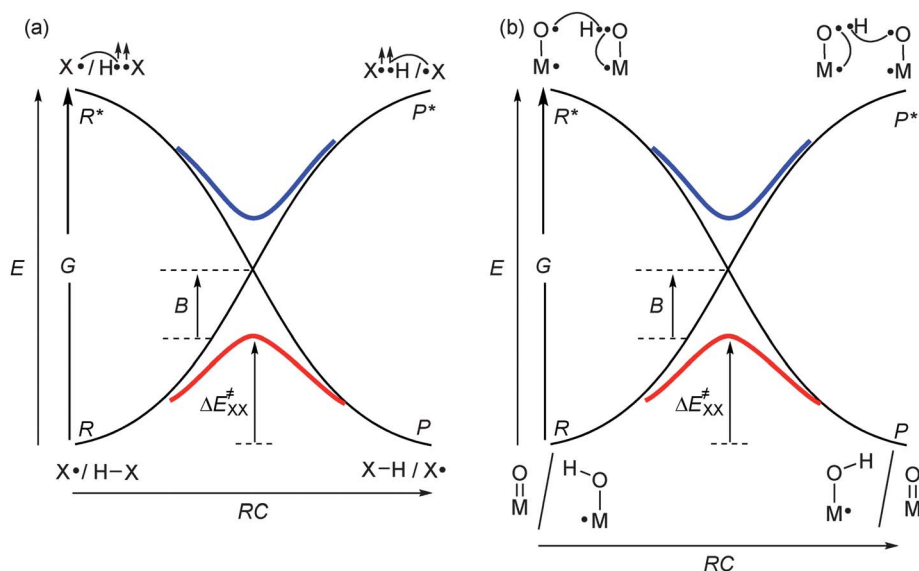


Fig. 5 VBSCDs describing normal HAT processes in identity reactions of, (a) a radical $X\cdot$ with an alkane $X-H$, and (b) a closed-shell abstractor $M=O$ ($M = Mn, Cr, C$) with a radical $\cdot M-OH$; G is the promotion energy gap (preparation energy) and B is the resonance energy of the TS; ΔE_{XX}^{\ddagger} is the general symbol for the barrier of identity reactions. The curved lines connecting the electron pairs signify singlet pairing.

$M=O$, where M can be Mn, Cr, C , etc. The curves are anchored in two ground states, R and P , of reactants and products, and two excited states, R^* and P^* . The excited states are the “prepared states” (or synonymously, the “promoted states”), which by crossing and mixing allow bonding changes and conversion from reactants to products along the reaction coordinate.^{21b,e} The state curves cross at the mid-point of the diagram and avoid the crossing by mixing, generating thereby the TS and barrier for the HAT process. The corresponding barrier^{21b,e,27} is given by eqn (3a):

$$\Delta E_{XX,VB}^{\ddagger} = fG - B_{XHX} \quad (3a)$$

$$f = 0.3 \quad (3b)$$

$$B_{XHX} = \frac{1}{2}BDE \quad (3c)$$

Thus, the barrier is a fraction f of the promotion energy gap G minus the avoided crossing term B . The quantity fG gauges the total deformation and repulsion energies of the reactants at the TS,³⁵ while B is the resonance energy of the TS due to the electronic delocalization. As shown before,²⁷ and indicated here in eqn (3a) and (3b), the value of f is 0.3 while B_{XHX} is one-half of the BDE of the bond $X-H$ that is broken and remade. The promotion energy G depends however, on the nature of the abstractor, whether it is a radical or a closed-shell molecule.

In Fig. 5a, the preparation of the R^* state involves de-coupling of the two bonding electrons of the $H-X$ bond to a triplet, and recoupling the electron on $H\cdot$ with the electron on the left-hand $X\cdot$. The promotion energy for this is given as twice the vertical bond energy, D , of the $H-X$ bond, in eqn (4a).^{21e,27} However, in the case of a hypothetical HAT for the closed-shell abstractor, the gap has to include the additional decoupling of $M=O$ bond, which converts it to an oxyl-radical moiety, $\cdot M-O\cdot$, that can

participate in H-abstraction.^{21b} The price for this additional preparation is proportional to the singlet–triplet excitation of the $M=O$ abstractor, as expressed in eqn (4b):

$$G(\text{open-shell}) = 2D_{HX} \quad (4a)$$

$$G(\text{closed-shell}) = 2D_{HO} + \frac{3}{4} \Delta E_{ST,M=O} \quad (4b)$$

$$D = BDE + |RE|_X \quad (4c)$$

The proportionality factor in eqn (4b) is 0.75 due to the spin pairing with the $H\cdot$ in the overall doublet $\cdot M-O\cdot/H$ species.³⁷

All the quantities in eqn (4a) and (4b) are accessible (see ESI†, Table S1 and S2), either from experimental data or from computations. D is obtained from the corresponding BDE , as expressed in eqn (4c), where $|RE|_X$ is the reorganization energy of the corresponding radical or abstractor. Thus for example, the reorganization energy of $CH_3\cdot$ is ~ 7 kcal mol⁻¹, which accounts for the geometry change of this moiety in the CH_3-H molecule as well as for the localization of the unpaired electron on the carbon atom. Delocalized radicals have much higher reorganization energies, e.g., 15.4 kcal mol⁻¹ for $DHA_{yl}\cdot$ and 12.5 kcal mol⁻¹ for $PhCH_2\cdot$ (see ESI†, Table S1). In the case of a closed-shell abstractor, e.g., of MnO_4^- , the reorganization energy is 18.6 kcal mol⁻¹, corresponding to the change in energy of the MnO_4^- moiety from its relaxed geometric and electronic structures to its state in the $MnO_3OH\cdot$ species. Analogous and even larger reorganization energies will appear in the barrier equations for the Cl_2CrO_2 and $(CH_3)_2C=O$ abstractors.

Thus, using all the relationships in eqn (3) and (4), we can write the final barriers expressions as follows:

$$\Delta E_{XX,VB}^{\ddagger}(\text{radical abstractor}) = 0.1BDE_{HX} + 0.6|RE|_X \quad (5a)$$

$$\Delta E_{XX,VB}^{\ddagger}(\text{MnO}_4^- \text{-abstractor}) = 0.1BDE_{HO} + 0.6|RE|_{M=O} + 0.225\Delta E_{ST,M=O} \quad (5b)$$

It is apparent from eqn (5a) and (5b), that the reorganization energy terms will make significant contributions to the identity barrier, and in the case of the closed-shell abstractor $M=O$ ($M = Mn, Cr, C, etc$), the additional preparation energy due to the singlet–triplet de-coupling of the $M=O$ bond will further contribute a substantial increment to the identity barrier in case of a HAT mechanism.

Eqn (5a) and (5b) allow us to estimate barriers from *raw* data, for specific identity reactions of radicals and closed-shell abstractors. The reactivity factors and VB-barriers are displayed in Table 4, alongside the directly computed DFT barriers. Let us focus initially on entries 1–9, which assume that all the reactions proceed *via* a normal HAT mechanism. Entries 1–6 correspond to HAT mechanisms by radicals, where we have added a few more reactions in order to demonstrate the predictive ability of the VBSCD model, while entries 7–9 involve an assumed HAT mechanism for closed-shell abstractors.

Inspection of entries 1–9 in Table 4 reveals that the VB model and eqn (5a) and (5b) for the HAT barrier predict nicely the DFT barriers for the reactions that involve radical abstractors. However, those VB barriers estimated for an *assumed* HAT mechanism, for the reactions of the closed-shell abstractors in entries 7–9, are highly overestimated compared with the DFT barriers. This is in line with the above expectations that the identity reactions of these closed-shell abstractors select in fact the more favorable PCET mechanism for abstracting the H atom.

VB modeling of PCET for identity reactions of closed-shell abstractors. As we argued by reference to Scheme 2 above, all the PCET mechanisms of oxo abstractors, such as ketones, MnO_4^- and Cl_2CrO_2 , contain four-electron/three-center $O\cdots H\cdots O$ moieties, whereas the unpaired electron, initially on the H-donor molecule, is delocalized between low-lying antibonding orbitals of the two moieties. We therefore need in addition to the HAT states in the VBSCDs in Fig. 5, also the charge transfer (CT) states that mediate the proton transfer (PT) event, and together constituting the PCET mechanism. This is shown in Fig. 6, using a generic abstractor $M=O$ ($M = Mn, Cr$ or C). Here we have two sets of VB curves in regular black for the normal HAT

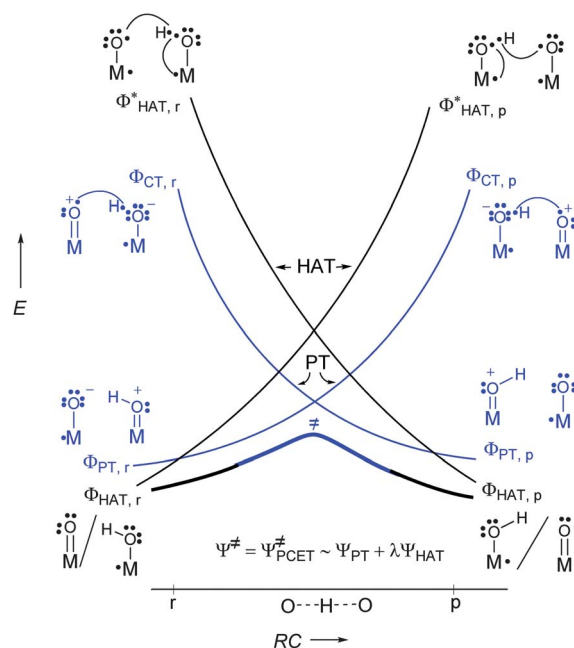


Fig. 6 VBSCD describing the PCET mechanism of the self H-exchange reaction $M=O + \cdot M-OH \rightarrow \cdot M-OH + M=O$, due to mixing and avoided crossing of normal HAT states (in black), and proton transfer (PT) states (in blue lines). Note that the character of the final energy profile (the bold curve) changes; it is PCET near the TS and it becomes HAT near reactants and products.

process and blue for the PT process. The CT promoted states for the blue state curves are generated by one-electron transfer from a lone-pair of the $M=O$: abstractor into the $O-H$ bond of $MO-H$. These blue VB curves correspond to the classical four-electron/three-center reactions that have been amply described in the past.^{21b,c,e} Thus, these PT VB-state curves are anchored in CT states of the reactants and products, $\Phi_{CT,r}$ and $\Phi_{CT,p}$, and correlate down to the corresponding proton-transferred reactants and products, which are higher than the corresponding HAT states that describe the reactants and products. Since the CT states lie below the crossing point of the HAT states, the

Table 4 Reactivity factors, VB derived barriers and DFT barriers ($kcal\ mol^{-1}$) for identity reactions

Reactions	<i>D</i>	<i>BDE</i>	<i>RE</i>	ΔE_{ST}	$\Delta E_{XX,VB}^e$	ΔE_{DFT}^f
(1) $CH_3\cdot/CH_4$	108.5	101.4	7.1		14.4	14.6
(2a) $C_6H_{11}\cdot/C_6H_{12}^a$	100.5	93.5	7.0		13.6	15.6
(2b) $C_6H_{11}\cdot/C_6H_{12}^a$	100.8	93.6	7.2		13.7	15.0
(3) $DHA_{y1}\cdot/DHA$	88.2	72.8	15.4		16.5	17.2
(4) allyl·/propene	99.5	82.6	16.9		18.4	19.4
(5) $C_6H_7\cdot/C_6H_8^b$	89.9	69.5	20.4		19.2	20.6
(6) $PhCH_2\cdot/PhCH_3$	97.8	85.3	12.5		16.0	16.5 ^g
(7) $Cl_2CrO_2/Cl_2CrO_2H\cdot$ (HAT) ^c	94.2	76.9	17.3	45.2	28.2	11.5
(8) $(CH_3)_2CO/(CH_3)_2COH\cdot$ (HAT) ^c	52.3	23.3	29.0	139.9	51.2	10.3
(9) $MnO_4^-/MnO_4^-H\cdot$ (HAT) ^c	95.8	77.2	18.6	34.8	26.7	11.6 (~15)
(10) $Cl_2CrO_2/Cl_2CrO_2H\cdot$ (PCET) ^d	94.2	76.9	17.3	45.2	13.4	11.5
(11) $(CH_3)_2CO/(CH_3)_2COH\cdot$ (PCET) ^d	53.3	23.3	30.0		15.4–17.7	10.3
(12) $MnO_4^-/MnO_4^-H\cdot$ (PCET) ^d	95.8	77.2	18.6		14.1	11.6 (~15)

^a Entry 2a corresponds to abstraction from the axial C–H, while entry 2b to the equatorial. ^b C_6H_8 is 1,4-cyclohexadiene. ^c Assumed to proceed *via* normal HAT mechanisms. ^d Assumed to proceed *via* PCET mechanisms. ^e Eqn (5a) and (5b) for entries 1–9, eqn (7) for entries 10–12. ^f For corresponding B3LYP/B2 data, see Table S3, ESI†. ^g From ref. 20a.

avoided crossing and mixing (no symmetry restrictions exist) of the four state curves generate a PCET-type TS, which involves a minor HAT character. However, on both extremes of the diagram, the ground states are dominated by the HAT states. As such, the mixing of four state curves creates a PCET TS that mediates a net HAT process.

The location of the charge transfer states with respect to the HAT state curves is affected at least by two factors. One factor is the steeper descent of the charge transfer states curves, which correspond to four-electron/three-center proton transfer and hence involving a strong triple ionic character, $O^- \cdots H^+ \cdots O^-$,^{21b,c,e} embedded in each of the state curves. This feature makes the curves highly concave, and hence they will likely cross the HAT curves below the crossing point of the latter, as described in fact in Fig. 6. The second factor is the location of the promoted CT states, at the extremes of the diagram. This location depends on the ionization energy (*IE*) of the abstractor and the electron affinity (*EA*) of the O–H bond. If we take for example, the case of the MnO_4^- abstractor, its *IE* should not be too high (our B3LYP/B1 *IE*[$MnO_4^-K^+$] value is 70 kcal mol⁻¹ lower than that of the lone pair of H₂O), while the electron affinity of MnO_3OH^- may well be substantial.³⁸ Therefore, to begin with, the charge transfer may lie below the HAT promoted states. These two factors taken together lower the CT state curves, which now dominate the TS region, and confer a PCET mechanism with a rather low barrier. Furthermore, since the proton transfer curves are anchored in CT states, unlike the HAT curves, their energy levels will be shifted by solvent effect. Hence, unlike HAT, the PCET reaction is expected to be sensitive to solvation.

An approximate way of evaluating the VB-barrier for the PCET mechanism in Fig. 6 considers the net promotion gap as the energy difference between the ground state on the reactant side (black line) all the way to the excited charge transfer state (blue line) on the product side. Viewed in this manner, the process involves breaking an MO–H bond, while at the same time creating a repulsive 3e-interaction between the H· species and the oxo electron pair of $\cdot M-O^-$ in the CT state. The repulsive three-electron interaction has the same expression as the corresponding bond strength.^{21b,c,e} Therefore the approximate value of this promotion energy gap is:

$$G_{PCET} \approx 2D_{OH} \quad (6)$$

One can see that the promotion gap for PCET does not involve anymore the additional energy for preparing the Mn=O for bonding by triplet decoupling. The VB barrier expression becomes:

$$\Delta E_{VB,PCET}^{\ddagger} \approx f_{av}(2D_{OH}) - \frac{1}{2}BDE_{OH}; f_{av} = (f_{HAT} + f_{PCET})/2 \approx 0.275 \quad (7)$$

Since the HAT and PCET curves mix, the fractional factor f_{av} is some average of corresponding factors for the two curve types. Being more concave, the f_{PCET} for the PCET curves is ~ 0.25 as in many four-electron/three-center reactions,^{21b,c,e;27d} which by averaging with $f_{HAT} = 0.3$, leads to $f_{av} = 0.275$. Using this value and the corresponding *D* and *BDE* values for the O–H bond for three different M=O abstractors, we estimated the PCET

barriers for the three identity reactions, which are shown in entries 10–12 in Table 4. It is apparent that the PCET barriers, in entries 10–12, are significantly lower by comparison to the corresponding barriers for the assumed HAT mechanism in entries 7–9. Furthermore, the PCET VB-barriers for MnO_4^-/MnO_3OH^- and $Cl_2CrO_2/Cl_2CrO_2H^-$ are close to the directly computed DFT barriers. The VB-barrier for $(CH_3)_2C=O/(CH_3)_2C-OH^-$ is still higher than the corresponding DFT barriers³⁹ but certainly much lower than the barrier in entry 8 which is calculated for an assumed HAT mechanism.

VB modeling of HAT/PCET for non-identity reactions. Fig. 7a shows the HAT and PCET state curves for a non-identity reaction between a generic closed shell abstractor, M=O, and an alkane H–Y, as those shown above in Table 1. Here, since the H–Y bond is a poor electron acceptor, the CT state curves lie higher than the corresponding HAT curves, and therefore the avoided crossing and VB mixing lead to a HAT TS, which will possess some variable PCET character due to the mixing of the PT states into the HAT TS, if no symmetry restrictions exist.

Fig. 7b shows a generic VBSCD for a non-identity reaction, with the necessary parameters for estimation of the barrier. As shown before,^{21d,e;27} the non-identity barrier can be estimated using the expression in eqn (8).

$$\Delta E_{VB}^{\ddagger} \approx 0.3G_0 + 0.5\Delta E_{rp} + 0.5[\Delta E_{rp}^2/G_0] - B_{XHY};$$

$$G_0 = 0.5(G_r + G_p)$$

$$B_{XHY} = \frac{1}{4}[BDE_{H-X} + BDE_{H-Y}] \quad (8)$$

Here, the promotion gap is an average of the corresponding gaps at the reactants and product side, and the *B* is also an average for the two interactions in the $X \cdots H \cdots Y$ TS.⁴⁰ Also, the reaction driving force ΔE_{rp} is seen to play a role in gauging the barrier height. Note that the expression treats the forward and reverse reaction on equal footing.

Using the HAT parameters in the VB expression in eqn (8), we can estimate the pure HAT barriers for the non-identity reactions studied here, with the expectation that the pure HAT equation will overestimate the barriers. The results are shown in Table 5. Inspection of entries 1–5 reveals that generally the VB model predicts the trend in the barriers very well and shows an apparent BEP behavior,³⁰ as found experimentally.^{15b–g,32c}

The VB barriers are closer to the closed-shell DFT barriers, in all cases. However, it is seen that for CH₄ and C₆H₁₂ with the strongest C–H bond, the VB barriers are within 2 kcal mol⁻¹ compared with the closed-shell DFT computed ones, while for the alkanes with the weaker C–H bonds in entries 3 and 4, the VB barrier is overestimated by 4–5 kcal mol⁻¹, compared with the DFT barriers. By comparison to the open-shell barriers, all VB barriers in entries 1–4 are overestimated by 5–6 kcal mol⁻¹. A larger overestimation is noted for the reaction of α -MS with DHA in entry 5. Since the VB model performs rather well for the HAT reactions of simple radicals, a plausible explanation for the above noted overestimation of the non-identity barriers is that the VB expression in eqn (8) corresponds to a pure HAT mechanism, and overestimates the barrier since it does not take into

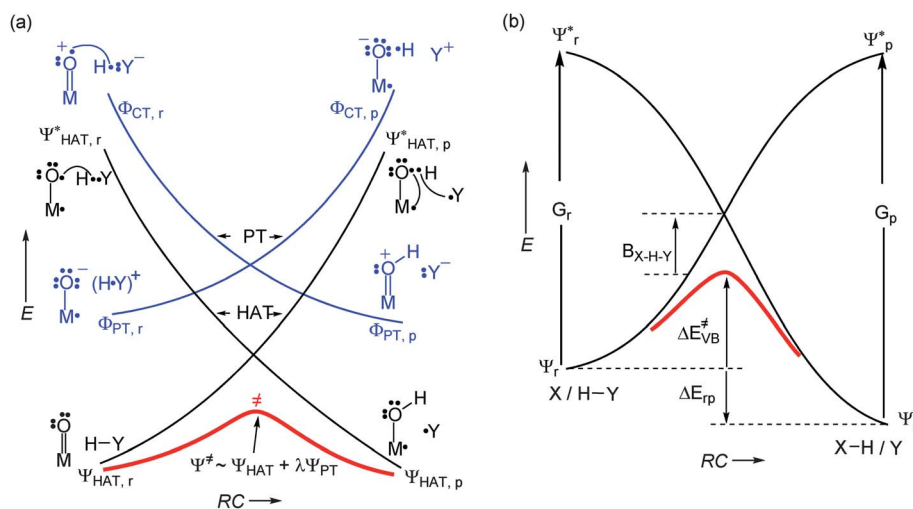


Fig. 7 (a) The VBSCD for a non-identity H-abstraction from an alkane H–Y by a closed-shell abstractor. (b) A generic VBSCD for non-identity reactions with corresponding reactivity parameters.

Table 5 Reactivity parameters (see Fig. 7b), and resulting VB barriers, shown alongside the DFT computed barriers (kcal mol⁻¹)

X	H–Y	G_0^a	ΔE_{TP}^b	B^a	$\Delta E_{\text{VB}}^{\ddagger}$	$\Delta E_{\text{B3LYP}}^{\ddagger c}$
(1) MnO ₄ ⁻	CH ₄	217.4	23.4	44.7	33.5	27.3/31.4
(2) MnO ₄ ⁻	C ₆ H ₁₂	209.4	16.4	42.7	29.0	23.3/27.3
(3) MnO ₄ ⁻	PhCH ₃	206.7	7.0	40.6	25.0	20.0/21.6
(4) MnO ₄ ⁻	DHA	197.1	-5.2	37.5	19.1	14.6/15.1
(5) α -MS	DHA	196.7	26.6	29.7	44.4	32.6/33.1

^a $G_0 = \frac{1}{2}(G_r + G_p)$; $G_r = 2D_{\text{CH}} + \frac{3}{4} \Delta E_{\text{ST},\text{X}}$, X = MnO₄⁻, α -MS, $G_p = 2D_{\text{XH}}$, $B = \frac{1}{4}(BDE_{\text{HX}} + BDE_{\text{HY}})$; see eqn (8). The values of D , BDE and ΔE_{ST} are B3LYP/B1 values collected in ESI†, Tables S1 and S2. ^b ΔE_{TP} are the ΔE (RC \rightarrow I_H) values from Table 1. ^c These are B3LYP/B1 values given in the order $\Delta E^{\ddagger}(\text{OS})/\Delta E^{\ddagger}(\text{CS})$; see Table 1.

account the secondary mixing of the CT state⁴¹ curves in Fig. 7a (mixing is possible since there is no symmetry restriction in these TS geometries). Mixing of these states into the HAT states will lower the barrier, in a manner depending on both the abstractor and the alkane. Thus, the $\Delta E_{\text{VB}}^{\ddagger} - \Delta E_{\text{B3LYP}}^{\ddagger}$ deviations may tentatively guide our understanding of the expected trends from the mixing of the CT states into the HAT states. This depends on two factors, which can be deduced from Fig. 7a:

(a) ΔE_{TP} : As the reaction becomes more endothermic, the TS of the HAT state-curves approaches the CT states, thereby causing increased mixing. Were this the only factor, we would expect more CT mixing as the C–H bond becomes stronger. This trend is apparent only for the highly endothermic reaction of α -MS and DHA in entry 5.

(b) The energy level of the $\Phi_{\text{CT},\text{r}}$ and $\Phi_{\text{CT},\text{p}}$ states on both sides of the diagram: As the CT states are lowered in energy they can mix more into the HAT TS.⁴¹ The $\Phi_{\text{CT},\text{r}}$ state energy depends on the electron affinity of the C–H bond in the alkane, while the $\Phi_{\text{CT},\text{p}}$ state energy depends on the IE of the Y· radical. Since the electron affinity of a bond increases as the bond becomes weaker,^{21b,c,e} and since the alkanes with the weak C–H bonds have also radicals with low IE , then changing the alkane, from CH₄ to C₆H₁₂ and then to PhCH₃ and DHA, will lower the

energy of both CT states and will increase their mixing with the HAT states, thereby lowering the barrier.

The factors in (b) anticipate that the CT mixing, in entries 1–4 of Table 5, should increase as the alkane varies from CH₄ with the strongest bond towards DHA. This seems to be the dominant trend if we consider the deviations between the VBSCD barriers and the closed-shell B3LYP barriers. However, considering the open-shell B3LYP barriers, the deviations are almost constant and fit better an opposing interplay between the factors in (a) and (b). In the case of the reaction of α -MS with DHA, both factors, (a) and (b), join to increase the CT mixing into the TS of the HAT states. Thus, the deviations $\Delta E_{\text{VB}}^{\ddagger} - \Delta E_{\text{B3LYP}}^{\ddagger}$ can be rationalized by the VBSCD to reflect a variable sampling of PCET character, due to mixing of the CT states into the HAT states, in the non-identity reaction series studied here.

Consequences of HAT/PCET blending. One outcome of this PCET/HAT blending is that the TSs of non-identity reactions sample different PCET characters, which vary with the nature of the abstractor and the alkane. A manifestation of this mechanistic blending could be our computational finding of a variable identity barrier extracted by the MCR analysis (eqn (2)) of a series of non-identity reactions of a single closed-shell abstractor, as shown for the MnO₄⁻/Y–H series (Table 3).

Fig. 8 summarizes the trends in the MCR extracted MnO₄⁻/MnO₃OH⁻ identity barrier, $\Delta E_{\text{XX}}^{\ddagger}$, from the various non-identity processes in Table 3. It is seen that no matter if we use closed-shell barrier or open-shell ones, the resulting $\Delta E_{\text{XX}}^{\ddagger}$ is variable. In the case of open-shell barriers, the value of the identity barrier decreases, as the C–H bond gets stronger, while usage of the closed-shell barriers results in an opposite trend. The horizontal red bars in Fig. 8 show the value of the directly computed B3LYP/B1 identity barrier for the PCET process (11.6 kcal mol⁻¹, see Tables 2–4). It is apparent that most of the MCR-identity barriers are higher than the value calculated directly for the PCET process, and the difference ranges between 5–10 kcal mol⁻¹. At the same time, these barriers are 6–12 kcal mol⁻¹ lower than the “pure” HAT value of 27.0 kcal mol⁻¹

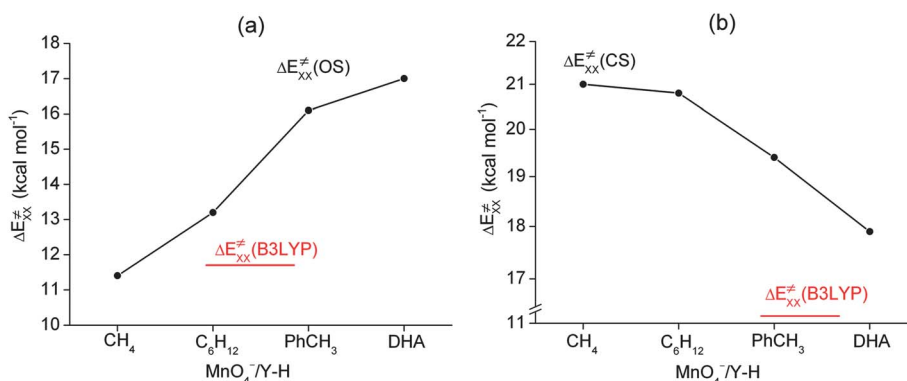


Fig. 8 $\text{MnO}_4^-/\text{MnO}_3\text{OH}^\cdot$ identity barriers (ΔE_{XX}^{\ddagger} , in kcal mol⁻¹) extracted by the MCR analysis (eqn (2)) of the B3LYP barriers in the $\text{MnO}_4^-/\text{Y-H}$ series ($\text{Y} = \text{CH}_3, \text{C}_6\text{H}_{11}, \text{PhCH}_2, \text{DHA}_y$). The lines connecting the data point serve to guide the eye. (a) $\Delta E_{XX}^{\ddagger}(\text{OS})$ values extracted from the open-shell barriers, and (b) $\Delta E_{XX}^{\ddagger}(\text{CS})$ values, using the closed-shell barriers, for the non-identity series.

determined from the VB expression eqn (8) (Table 4, entries 7–9). Based on the VBSCD analysis (Fig. 7a), this variable ΔE_{XX}^{\ddagger} value represents the *variable* mixing of the CT states into the HAT states, and hence a variable sampling of PCET character.

The ΔE_{XX}^{\ddagger} trend in Fig. 8a fits the above-discussed effect of reaction endothermicity. Thus, as the C–H bond gets stronger the HAT states are raised, and this should cause greater mixing of the charge transfer states into the HAT TS, resulting in a lower MCR-based ΔE_{XX}^{\ddagger} . On the other hand, the ΔE_{XX}^{\ddagger} trend in Fig. 8b fits the second factor discussed above, namely the impact of the energy level of the CT states at the diagram extremes. Thus, as the C–H bond gets weaker and the IE_Y is lowered, the CT states will be lowered and will mix more into the HAT states leading to increased PCET character as the alkane varies from CH₄ sequentially to DHA. The available experimental data for the reactions of MnO_4^- and Cl_2CrO_2 with alkanes (Table 2, entries 4 and 5), indicate the latter trend: thus the MCR analyses of the experimental barriers suggests that when the C–H bond is weak (*e.g.*, DHA and PhCH₃) the resulting ΔG_{XX}^{\ddagger} values are small, while when the C–H bond is strong (*e.g.*, C₆H₁₂), the ΔG_{XX}^{\ddagger} value is high.

Furthermore, when the identity reaction itself is a pure HAT, such as for α -MS abstracting a hydrogen from the cumyl radical, the MCR-extracted identity barrier from a series of non-identity reactions will be smaller than the one computed or experimentally determined directly for the identity reaction, thus reflecting the *mixing* of the charge transfer states into the HAT states. Indeed, as can be seen from entry 7 in Table 2, the identity barrier of α -MS/cumyl \cdot extracted by the MCR analysis of the experimental enthalpy of activation for the reaction^{15h} of α -MS with DHA is 15.6 kcal mol⁻¹, and similar values are obtained from MCR analysis of the B3LYP barriers, 16.6/17.8 kcal mol⁻¹ (from entry 5 in Table 3), while the directly calculated DFT barrier for the actual process (which corresponds to HAT) is 23.2 kcal mol⁻¹. The blending of PCET character in this HAT process is quite apparent.

Another interesting feature, which is apparent from Fig. 8 is that nearly all the MCR-identity barriers for the $\text{MnO}_4^-/\text{MnO}_3\text{OH}^\cdot$ pair are higher than the directly determined barrier (11.6 kcal mol⁻¹) that corresponds to the PCET mechanism. These higher identity barriers reflect the additional “preparation

energy” required to decouple the electrons of the Mn=O bond so it can participate in a HAT process, as described in the VBSCD in Fig. 5b. Thus, the series of MCR extracted $\text{MnO}_4^-/\text{MnO}_3\text{OH}^\cdot$ identity barriers project nicely, that closed-shell abstractors pay a price to abstract hydrogen atom, a price which open-shell abstractors do not have to pay.^{9,10,12,13} This is a general conclusion and is expected for other closed-shell abstractors, as indeed reported recently for vanadium(v)-oxo complexes,¹⁸ and the earlier findings about the singlet states of Mn(v)-oxo complexes.^{13a,b,17}

Concluding remarks

The present study investigates the mechanisms of H-abstraction for 15 self H-exchange (identity and non-identity) reactions of radical and closed-shell abstractors, which were studied experimentally.^{15,31–33} All these reactions were then subjected to a MCR analysis²² to extract intrinsic barriers and resolve them into their component-identity barriers. Subsequently, the reactions were analyzed using the VB diagram model,^{21,27} which enables one to estimate H-abstraction barriers from raw data.

A key goal of the study was to answer the question, “is it *necessary* to have a radical center at the abstractor in order to abstract a hydrogen atom”? The answer to this question is, “*of course not*”, but if the abstractor is a closed-shell molecule then in the normal HAT event, this will require a high barrier due to the additional preparation energy that is required in order to *create* radical and prepare the abstractor for H-abstraction (Fig. 5a vs. 5b; eqn (5a) and (5b)). This energy penalty for closed-shell abstractions is apparent in the present computational data, as well as in experimental systems.^{13a,b,15,17,18}

The computational study has further revealed that small barriers for closed-shell abstractors are encountered whenever the abstractor has a way to avoid this excess promotion energy while at the same time abstracting a hydrogen species. This is achieved *via* the alternative path of concerted PCET, whereby a proton is abstracted by the basic moiety of the abstractor, while an electron is being transferred through orbitals not involved in the proton abstraction region. PCET mechanisms were found for all the identity reactions of the closed-shell oxo abstractors, *e.g.*, $\text{MnO}_4^-/\text{MnO}_3\text{OH}^\cdot$ and $\text{Cl}_2\text{CrO}_2/\text{Cl}_2\text{CrO}_2\text{H}^\cdot$. However, the

corresponding non-identity reactions of MnO_4^- with alkanes Y-H ($\text{Y} = \text{CH}_3, \text{C}_6\text{H}_{11}, \text{PhCH}_2, \text{DHA}_{\text{yl}}$) revealed that the transition states are clearly HAT types (Fig. 4), albeit with some variable PCET characters as reflected by the group charges.

The MCR analysis (eqn (2a) and (2b)) of the non-identity barriers for $\text{X} = \text{MnO}_4^-$ reacting with alkanes Y-H ($\text{Y} = \text{CH}_3, \text{C}_6\text{H}_{11}, \text{PhCH}_2, \text{DHA}_{\text{yl}}$) produced also identity barriers for the $\text{MnO}_4^-/\text{MnO}_3\text{OH}^-$ identity reaction, which differed from one reaction to the other, depending on the C–H bond strength of the alkane used in the non-identity reaction. The VB modeling of the H-abstraction process revealed the importance of the mixed HAT/PCET spectrum. As shown by the VB analysis, these non-identity reactions *sample* PCET characters that depend on the C–H bond strength of the alkane, and hence will cause the MCR analysis to produce different identity barriers for the same identity reaction. This can be a probe of HAT/PCET blending.

The VB formulation of the HAT/PCET mechanistic blending is shown to be predictive and insightful. Such insight and predictive ability are typical to VB modeling,^{23,42–47} and related energy-decomposition approaches,³⁵ of chemical reactivity.

Acknowledgements

The research is supported by the Israeli Science Foundation (ISF grant 09/53), and by a special Minerva Grant. We are thankful to D. Dinnocenzo and M. Danovich for careful checking of kinetic data used herein.

Notes and references

- Biomimetic Oxidations Catalyzed by Transition Metal Complexes*, ed. B. Meunier, Imperial College Press, London, 2000.
- For HAT in P450, see: (a) P. R. Ortiz de Montellano, *Chem. Rev.*, 2010, **110**, 932; (b) J. T. Groves, *J. Chem. Educ.*, 1985, **62**, 928.
- For recent theoretical treatments of HAT by P450s, see: (a) K. Yoshizawa, *Coord. Chem. Rev.*, 2002, **226**, 251; (b) S. Shaik, S. Cohen, Y. Wang, H. Chen, D. Kumar and W. Thiel, *Chem. Rev.*, 2010, **110**, 949.
- HAT is important for plants: (a) H. B. Dunford, *Heme Peroxidases*, Wiley-VCH, New York, 1999; (b) H. U. Markwalder and H. Neukom, *Phytochemistry*, 1976, **15**, 836.
- (a) J. Hioe and H. Zipse, *Faraday Discuss.*, 2010, **145**, 301; (b) J. Stubbe and W. A. van der Donk, *Chem. Rev.*, 1998, **98**, 705.
- For computational studies of radical enzymes, see for example: (a) F. Himo, *Biochim. Biophys. Acta, Bioenerg.*, 2005, **1707**, 24; (b) F. Himo and P. E. M. Siegbahn, *Chem. Rev.*, 2003, **103**, 2421; (c) F. Himo and L. A. Eriksson, *J. Am. Chem. Soc.*, 1998, **120**, 11449.
- For HAT in non-heme systems, see for example: (a) C. Krebs, D. G. Fujimori, C. T. Walsh and J. M. Bollinger, Jr, *Acc. Chem. Res.*, 2007, **40**, 484; (b) W. Nam, *Acc. Chem. Res.*, 2007, **40**, 522; (c) G. Q. Xue, R. De Hont, E. Münck and L. Que, Jr., *Nat. Chem.*, 2010, **2**, 400; (d) P. H. Buist, *Nat. Prod. Rep.*, 2004, **21**, 249.
- For synthetic non-heme complexes and their HAT reactions, see: (a) J.-U. Rohde, J.-H. In, M. H. Lim, W. W. Brennessel, M. R. Bukowski, A. Stubna, E. Münck, W. Nam and L. Que, Jr., *Science*, 2003, **299**, 1037; (b) J. Kaizer, E. J. Klinker, N. Y. Oh, J.-U. Rohde, W. J. Song, A. Stubna, J. Kim, E. Münck, W. Nam and L. Que, Jr., *J. Am. Chem. Soc.*, 2004, **126**, 472; (c) P. Comba, S. Fukuzumi, H. Kotani and S. Wunderlich, *Angew. Chem., Int. Ed.*, 2010, **49**, 2622.
- For HAT by diatomic cations, see for example: (a) D. Schröder and H. Schwarz, *Angew. Chem., Int. Ed. Engl.*, 1995, **34**, 1973; (b) H. Schwarz, *Int. J. Mass Spectrom.*, 2004, **237**, 75; (c) N. Dietl, C. van der Linde, M. Schlangen, M. K. Beyer and H. Schwarz, *Angew. Chem., Int. Ed.*, 2011, **50**, 4966.
- For some recent reviews, see: (a) D. Balcells, E. Clot and O. Eisenstein, *Chem. Rev.*, 2010, **110**, 749; (b) J. Roithová and D. Schröder, *Chem. Rev.*, 2010, **110**, 1170; (c) C. Copéret, *Chem. Rev.*, 2010, **110**, 656; (d) T. Newhouse and P. S. Baran, *Angew. Chem., Int. Ed.*, 2011, **50**, 3362.
- For atmospheric HAT, see: J. S. Francisco and M. M. Maricq, *Acc. Chem. Res.*, 1996, **29**, 391, and references therein.
- A. A. Fokin and P. R. Schreiner, *Chem. Rev.*, 2002, **102**, 1551.
- See for example, metallo-oxyl radical characters: (a) D. Balcells, C. Raynaud, R. H. Crabtree and O. Eisenstein, *Inorg. Chem.*, 2008, **47**, 10090; (b) D. Balcells, C. Raynaud, R. H. Crabtree and O. Eisenstein, *Chem. Commun.*, 2008, 744; (c) S. F. Ye and F. Neese, *Proc. Natl. Acad. Sci. U. S. A.*, 2011, **108**, 1228; (d) E. I. Solomon, S. D. Wong, L. V. Liu, A. Decker and M. S. Chow, *Curr. Opin. Chem. Biol.*, 2009, **13**, 99.
- For the importance of oxyl radical, see: (a) K. Chen, Z.-C. Wang, M. Schlangen, Y.-D. Wu, X. H. Zhang and H. Schwarz, *Chem.–Eur. J.*, 2011, **17**, 9619; (b) N. Dietl, M. Engeser and H. Schwarz, *Angew. Chem., Int. Ed.*, 2009, **48**, 4861; (c) D. Schröder and J. Roithová, *Angew. Chem., Int. Ed.*, 2006, **45**, 5705; (d) A. Božović and D. K. Bohme, *Phys. Chem. Chem. Phys.*, 2009, **11**, 5940.
- For reactions of closed-shell abstractors, see: (a) K. B. Wiberg and G. Foster, *J. Am. Chem. Soc.*, 1961, **83**, 423; (b) K. B. Wiberg and R. Eisenthal, *Tetrahedron*, 1964, **20**, 1151; (c) G. K. Cook and J. M. Mayer, *J. Am. Chem. Soc.*, 1994, **116**, 1855; (d) G. K. Cook and J. M. Mayer, *J. Am. Chem. Soc.*, 1995, **117**, 7139; (e) K. A. Gardner and J. M. Mayer, *Science*, 1995, **269**, 1849; (f) J. M. Mayer, *Acc. Chem. Res.*, 1998, **31**, 441; (g) for reactions of MnO_4^- , see: K. A. Gardner, L. L. Kuehnert and J. M. Mayer, *Inorg. Chem.*, 1997, **36**, 2069; (h) C. Rüchardt, M. Gerst and M. Nöltke, *Angew. Chem., Int. Ed. Engl.*, 1992, **31**, 1523; (i) C. Limberg, *Chem.–Eur. J.*, 2000, **6**, 2083; (j) P. J. Wagner, Y. Zhang and A. E. Puchalski, *J. Phys. Chem.*, 1993, **97**, 13368.
- (a) K. A. Prokop, S. P. de Visser and D. P. Goldberg, *Angew. Chem., Int. Ed.*, 2010, **49**, 5091; (b) T. Kojima, Y. Hirai, T. Ishizuka, Y. Shiota, K. Yoshizawa, K. Ikemura, T. Ogura and S. Fukuzumi, *Angew. Chem., Int. Ed.*, 2010, **49**, 8449; (c) D. Schröder and S. Shaik, *Angew. Chem., Int. Ed.*, 2011, **50**, 3850; (d) T. Kojima and S. Fukuzumi, *Angew. Chem., Int. Ed.*, 2011, **50**, 3852.
- (a) N. Jin and J. T. Groves, *J. Am. Chem. Soc.*, 1999, **121**, 2923; (b) N. Jin, J. L. Bourassa, S. C. Tizio and J. T. Groves, *Angew. Chem., Int. Ed.*, 2000, **39**, 3849; (c) F. De Angelis, N. Jin, R. Car and J. T. Groves, *Inorg. Chem.*, 2006, **45**, 4268.
- C. R. Waidmann, X. Zhou, E. A. Tsai, W. Kaminsky, D. A. Hrovat, W. T. Borden and J. M. Mayer, *J. Am. Chem. Soc.*, 2009, **131**, 4729.
- For some general references on PCET mechanisms, see: (a) R. I. Cukier and D. G. Nocera, *Annu. Rev. Phys. Chem.*, 1998, **49**, 337; (b) J. M. Mayer, *Annu. Rev. Phys. Chem.*, 2004, **55**, 363; (c) M. H. V. Huynh and T. J. Meyer, *Chem. Rev.*, 2007, **107**, 5004; For PCET/HAT relationships see: (d) J. H. Skone, A. V. Soudackov and S. Hammes-Schiffer, *J. Am. Chem. Soc.*, 2006, **128**, 16655; (e) O. Tishchenko, D. G. Truhlar, A. Ceulemans and M. T. Nguyen, *J. Am. Chem. Soc.*, 2008, **130**, 7000; (f) For PCET in PS II, see: P. E. M. Siegbahn, *Acc. Chem. Res.*, 2009, **42**, 1871; (g) C. Costentin, M. Robert and J.-M. Savéant, *Acc. Chem. Res.*, 2010, **43**, 1019; (h) O. S. Wenger, *Chem.–Eur. J.*, 2011, **17**, 11692; (i) S. B. Liu, D. H. Ess and C. K. Schauer, *J. Phys. Chem. A*, 2011, **115**, 4738.
- (a) J. M. Mayer, D. A. Hrovat, J. L. Thomas and W. T. Borden, *J. Am. Chem. Soc.*, 2002, **124**, 11142; (b) M. Lingwood, J. R. Hammond, D. A. Hrovat, J. M. Mayer and W. T. Borden, *J. Chem. Theory Comput.*, 2006, **2**, 740.
- (a) S. S. Shaik, *J. Am. Chem. Soc.*, 1981, **103**, 3692; (b) S. Shaik and A. Shurki, *Angew. Chem., Int. Ed.*, 1999, **38**, 586; (c) S. Shaik and P. C. Hiberty, *A Chemist's Guide to Valence Bond Theory*, John Wiley & Sons Inc., New York, 2008; (d) A. Pross, *Theoretical and Physical Principles of Organic Reactivity*, John Wiley & Sons, Inc., New York, 1995; (e) W. Z. Lai, C. S. Li, H. Chen and S. Shaik, *Angew. Chem., Int. Ed.*, 2012, **51**, DOI: 10.1002/anie.201108398.
- R. A. Marcus, *J. Am. Chem. Soc.*, 1969, **91**, 7224.
- For an extended MCR analysis and LEPS modeling of hydrid transfer of ca. 50 reactions, see: Y. Kim, D. G. Truhlar and M. M. Kreevoy, *J. Am. Chem. Soc.*, 1991, **113**, 7837.
- (a) A. D. Becke, *Phys. Rev. A: At., Mol., Opt. Phys.*, 1988, **38**, 3098; (b) A. D. Becke, *J. Chem. Phys.*, 1993, **98**, 5648; (c) C. T. Lee, W. T. Yang and R. G. Parr, *Phys. Rev. B*, 1988, **37**, 785.

- 25 (a) M. J. Frisch, G. W. Trucks, H. B. Schlegel, G. E. Scuseria, M. A. Robb, J. R. Cheeseman, G. Scalmani, V. Barone, B. Mennucci, G. A. Petersson, H. Nakatsuji, M. Caricato, X. Li, H. P. Hratchian, A. F. Izmaylov, J. Bloino, G. Zheng, J. L. Sonnenberg, M. Hada, M. Ehara, K. Toyota, R. Fukuda, J. Hasegawa, M. Ishida, T. Nakajima, Y. Honda, O. Kitao, H. Nakai, T. Vreven, J. A. Montgomery, Jr., J. E. Peralta, F. Ogliaro, M. Bearpark, J. J. Heyd, E. Brothers, K. N. Kudin, V. N. Staroverov, R. Kobayashi, J. Normand, K. Raghavachari, A. Rendell, J. C. Burant, S. S. Iyengar, J. Tomasi, M. Cossi, N. Rega, J. M. Millam, M. Klene, J. E. Knox, J. B. Cross, V. Bakken, C. Adamo, J. Jaramillo, R. Gomperts, R. E. Stratmann, O. Yazyev, A. J. Austin, R. Cammi, C. Pomelli, J. Ochterski, R. L. Martin, K. Morokuma, V. G. Zakrzewski, G. A. Voth, P. Salvador, J. J. Dannenberg, S. Dapprich, A. D. Daniels, O. Farkas, J. B. Foresman, J. V. Ortiz, J. Cioslowski and D. J. Fox, *GAUSSIAN 09 (Revision B.01)*, Gaussian, Inc., Wallingford, CT, 2010; (b) E. D. Glendening, J. K. Badenhop, A. E. Reed, J. E. Carpenter, J. A. Bohmann, C. M. Morales and F. Weinhold, *NBO 5.0*, Theoretical Chemistry Institute, University of Wisconsin, Madison, WI, 2004.
- 26 (a) For basis sets 6-311++G**, see: A. D. McLean and G. S. Chandler, *J. Chem. Phys.*, 1980, **72**, 5639; R. Krishnan, J. S. Binkley, R. Seeger and J. A. Pople, *J. Chem. Phys.*, 1980, **72**, 650; J.-P. Blaudeau, M. P. McGrath, L. A. Curtiss and L. Radom, *J. Chem. Phys.*, 1997, **107**, 5016; A. J. H. Wachters, *J. Chem. Phys.*, 1970, **52**, 1033; P. J. Hay, *J. Chem. Phys.*, 1977, **66**, 4377; K. Raghavachari and G. W. Trucks, *J. Chem. Phys.*, 1989, **91**, 1062; (b) for basis set Def2-TZVP, see: F. Weigend, M. Häser, H. Patzelt and R. Ahlrichs, *Chem. Phys. Lett.*, 1998, **294**, 143; F. Weigend and R. Ahlrichs, *Phys. Chem. Chem. Phys.*, 2005, **7**, 3297; (c) for basis sets aug-cc-pVTZ and aug-cc-pVQZ used in CCSD(T), see: R. A. Kendall, T. H. Dunning, Jr. and R. J. Harrison, *J. Chem. Phys.*, 1992, **96**, 6796; D. E. Woon and T. H. Dunning, Jr., *J. Chem. Phys.*, 1993, **98**, 1358.
- 27 (a) P. F. Su, L. C. Song, W. Wu, P. C. Hiberty and S. Shaik, *J. Am. Chem. Soc.*, 2004, **126**, 13539; (b) L. C. Song, W. Wu, K. M. Dong, P. C. Hiberty and S. Shaik, *J. Phys. Chem. A*, 2002, **106**, 11361; (c) S. Shaik, D. Kumar and S. P. de Visser, *J. Am. Chem. Soc.*, 2008, **130**, 10128; (d) S. Shaik, W. Z. Lai, H. Chen and Y. Wang, *Acc. Chem. Res.*, 2010, **43**, 1154.
- 28 A. J. Johansson, M. R. A. Blomberg and P. E. M. Siegbahn, *J. Phys. Chem. C*, 2007, **111**, 12397.
- 29 T. Strassner and K. N. Houk, *J. Am. Chem. Soc.*, 2000, **122**, 7821.
- 30 (a) R. P. Bell, *Proc. R. Soc. London, Ser. A*, 1936, **154**, 414; (b) M. G. Evans and M. Polanyi, *Trans. Faraday Soc.*, 1938, **34**, 11.
- 31 (a) For the identity barrier of $\text{CH}_3\cdot/\text{CH}_4$ see: G. A. Creak, F. S. Dainton and K. J. Ivin, *Trans. Faraday Soc.*, 1962, **58**, 326; (b) A $\Delta G^\ddagger(300\text{ K}) \approx 20\text{ kcal mol}^{-1}$ datum can be estimated from the data in F. S. Dainton, K. J. Ivin and F. Wilkinson, *Trans. Faraday Soc.*, 1959, **55**, 929.
- 32 (a) J. R. Bryant, *Mechanistic Studies of the Oxidations by Manganese and Ruthenium Transition Metal Complexes*, PhD Thesis, The University of Washington, Seattle, WA, 2002, p. 82; (b) J. J. Warren and J. M. Mayer, *Proc. Natl. Acad. Sci. U. S. A.*, 2010, **107**, 5282 and the SI for the paper; (c) J. M. Mayer, *Acc. Chem. Res.*, 2011, **44**, 36; (d) J. J. Warren, T. A. Tronic and J. M. Mayer, *Chem. Rev.*, 2010, **110**, 6961.
- 33 For $\text{PhCH}_2\cdot/\text{PhCH}_3$ see: R. A. Jackson and D. W. O'Neal, *J. Chem. Soc. D*, 1969, 1210 ($\Delta H^\ddagger \approx 18.7$ and $\Delta G^\ddagger(298\text{ K}) \approx 23.4\text{ kcal mol}^{-1}$).
- 34 (a) For an explanation using an MO-CI perspective, see: W. T. Borden, *Modern Molecular Orbital Theory for Organic Chemists*, Prentice-Hall, Inc., Englewood Cliffs, NJ, 1975, pp. 265–271; (b) for a recent VB perspective, see: Y. Luo, L. C. Song, W. Wu, D. Danovich and S. Shaik, *ChemPhysChem*, 2004, **5**, 515.
- 35 (a) G. T. de Jong and F. M. Bickelhaupt, *ChemPhysChem*, 2007, **8**, 1170; (b) B. Braida, C. Walter, B. Engels and P. C. Hiberty, *J. Am. Chem. Soc.*, 2010, **132**, 7631; (c) D. H. Ess and K. N. Houk, *J. Am. Chem. Soc.*, 2008, **130**, 10187; (d) K. Kitaura and K. Morokuma, *Int. J. Quantum Chem.*, 1976, **10**, 325; (e) T. Ziegler and A. Rauk, *Inorg. Chem.*, 1979, **18**, 1558; (f) F. M. Bickelhaupt and E. J. Baerends, *Rev. Comput. Chem.*, 2000, **15**, 1; (g) for a related approach that extract VB information from MO and DFT computations, see: Y. R. Mo and S. D. Peyerimhoff, *J. Chem. Phys.*, 1998, **109**, 1687; Y. R. Mo and J. L. Gao, *J. Comput. Chem.*, 2000, **21**, 1458.
- 36 H. Isobe, S. Yamanaka, M. Okumura, K. Yamaguchi and J. Shimada, *J. Phys. Chem. B*, 2011, **115**, 10730.
- 37 The direct correlation of the states leads to $G = 0.75\Delta E_{\text{ST}}$. See ref. 21d, pp. 141–144.
- 38 G. V. Ionova and M. E. Dyatkina, *Zh. Strukt. Khim.*, 1965, **6**, 796.
- 39 If the TS of this reaction maintains a plane of symmetry then, the TS is a pure PCET type, and the corresponding f factor to be used is 0.25, leading to a barrier of 15 kcal mol^{-1} .
- 40 For use of the averaged B expression, see eqn 3.26 in S. Shaik and P. C. Hiberty, in *Advances in Quantum Chemistry*, ed. P. O. Lowdin, J. R. Sabin and M. C. Zerner, Elsevier Academic Press Inc, San Diego, CA, 1995, vol. 26, p. 99.
- 41 S. Shaik, P. Milko, P. Schyman, D. Usharani and H. Chen, *J. Chem. Theory Comput.*, 2011, **7**, 327.
- 42 The empirical VB (EVB) model is the basis of understanding and modeling enzymatic reactions, see e.g., (a) A. Warshel and R. M. Weiss, *J. Am. Chem. Soc.*, 1980, **102**, 6218; (b) J. Åqvist and A. Warshel, *Chem. Rev.*, 1993, **93**, 2523.
- 43 For a recent VB coupled with QM/MM, see: (a) A. Sharir-Ivry, H. A. Crown, W. Wu and A. Shurki, *J. Phys. Chem. A*, 2008, **112**, 2489; (b) A. Shurki and H. A. Crown, *J. Phys. Chem. B*, 2005, **109**, 23638.
- 44 B. Braida, V. Prana and P. C. Hiberty, *Angew. Chem., Int. Ed.*, 2009, **48**, 5724.
- 45 (a) M.-D. Su and S.-Y. Chu, *Inorg. Chem.*, 1998, **37**, 3400; (b) M.-D. Su and S.-Y. Chu, *J. Am. Chem. Soc.*, 1997, **119**, 10178; (c) M.-D. Su, *Inorg. Chem.*, 1995, **34**, 3829.
- 46 (a) Y. S. Wang, O. Haze, J. P. Dinnocenzo, S. Farid, R. S. Farid and I. R. Gould, *J. Phys. Chem. A*, 2008, **112**, 13088; (b) Y. S. Wang, O. Haze, J. P. Dinnocenzo, S. Farid, R. S. Farid and I. R. Gould, *J. Org. Chem.*, 2007, **72**, 6970.
- 47 H. Zipse, *Acc. Chem. Res.*, 1999, **32**, 571.